

CHARACTERIZING THE COOL KOIS VIII. PARAMETERS OF THE PLANETS ORBITING KEPLER'S COOLEST DWARFS

JONATHAN J. SWIFT^{1,*}, BENJAMIN T. MONTET^{1,2}, ANDREW VANDERBURG², TIMOTHY MORTON³, PHILIP S. MUIRHEAD⁴, JOHN ASHER JOHNSON²

(Dated: Thursday 4th April, 2024, 22:34)
Draft version Thursday 4th April, 2024

ABSTRACT

The coolest dwarf stars targeted by the *Kepler* Mission constitute a relatively small but scientifically valuable subset of the *Kepler* target stars, and provide a high-fidelity and nearby sample of transiting planetary systems. Using archival *Kepler* data spanning the entire primary mission we perform a uniform analysis to extract, confirm and characterize the transit signals discovered by the *Kepler* pipeline toward M-type dwarf stars. We recover all but two of the signals reported in a recent listing from the Exoplanet Archive resulting in 165 planet candidates associated with a sample of 106 low-mass stars. We fitted the observed light curves to transit models using Markov Chain Monte Carlo and we have made the posterior samples publicly available to facilitate further studies. We fitted empirical transit times to individual transit signals with significantly non-linear ephemerides for accurate recovery of transit parameters and measuring precise transit timing variations. We also provide the physical parameters for the stellar sample, including new measurements of stellar rotation, allowing the conversion of transit parameters into planet radii and orbital parameters.

Subject headings: stars: late-type — stars: low-mass — planets and satellites

1. INTRODUCTION

NASA's *Kepler* Space Mission was designed to monitor more than 150,000 stars within a single 115 square degree patch of sky in search of periodic diminutions of light caused by transiting exoplanets (Borucki et al. 2010; Koch et al. 2010; Jenkins et al. 2010). *Kepler*'s great success in discovering transiting exoplanets (Borucki et al. 2011a,b; Batalha et al. 2013; Burke et al. 2014) has revealed that planets are at least as numerous as stars in the Galaxy (Fressin et al. 2013; Petigura et al. 2013a; Swift et al. 2013; Dressing & Charbonneau 2013; Morton & Swift 2014). Beyond the sheer numbers of planets, *Kepler* has also provided important insights into the characteristics of the transiting planet population. The multi-transit systems reveal highly coplanar multi-planet systems (Lissauer et al. 2011b; Tremaine & Dong 2012; Fang & Margot 2012; Fabrycky et al. 2014; Ballard & Johnson 2014), many of which are in compact configurations (*e.g.* Lissauer et al. 2011a; Muirhead et al. 2012b; Swift et al. 2013). The period ratios of adjacent transiting planets show an excess just outside of mean motion resonance (Lissauer et al. 2011b; Fabrycky et al. 2014) that may reflect the mechanisms by which these systems formed (Rein 2012; Goldreich & Schlichting 2014), or else may indicate subsequent evolution of these systems (Lithwick & Wu 2012; Batygin & Morbidelli 2013). The typical surface density profile of the protoplanetary disks

from which these planets formed can be estimated using the *Kepler* sample, and implies that either protoplanetary disks contain a large amount of material within ~ 0.1 AU of the host star (Chiang & Laughlin 2013; Hansen & Murray 2012) or that the planets migrated from their birth places further out in the disk (Swift et al. 2013; Schlichting 2014). Another clue regarding the formation mechanisms behind the *Kepler* planet sample is the radius function—the frequency of planets as a function of their size—that shows unambiguously that there are many more planets with radii less than that of Neptune than there are larger ones (Howard et al. 2012; Fressin et al. 2013; Petigura et al. 2013b; Morton & Swift 2014; Foreman-Mackey et al. 2014).

Although the vast majority of *Kepler* target stars are Sun-like ($0.8 M_{\odot} \lesssim M_{\star} \lesssim 1.2 M_{\odot}$), several thousand M dwarfs have been monitored by *Kepler* over the course of the primary mission. The initial photometric characterization of the M dwarfs in the *Kepler* field was known to be inaccurate because the the *Kepler* Input Catalog was optimized for Sun-like stars (KIC; Brown et al. 2011). However, there have been several efforts to revise the stellar parameters for this sample (*e.g.* Muirhead et al. 2012b; Mann et al. 2012, 2013; Dressing & Charbonneau 2013; Muirhead et al. 2014; Newton et al. 2014). Since the physical parameters of a transiting planet are dependent on the stellar parameters, many exciting results have come from a careful examination of this stellar sample (*e.g.* Johnson et al. 2011a, 2012; Muirhead et al. 2012a, 2013). The depth of a transit signal is proportional to the square of the relative planet radius, $\delta \propto (R_p/R_{\star})^2$ allowing the detection of smaller planets around these smaller stars. This higher sensitivity to smaller planets allows the planet population around *Kepler*'s M dwarfs to be well-sampled down to $\lesssim 1 R_{\oplus}$, where planets are most prevalent (Morton & Swift 2014). Further, the notional “habitable zone”, in which planets

¹ California Institute of Technology, 1200 E. California Blvd., Pasadena, CA 91125 USA

^{*} Current address: The Thacher School, 5025 Thacher Rd., Ojai, CA 93023

² Harvard-Smithsonian Center for Astrophysics, Cambridge, MA 02138 USA

³ Department of Astrophysical Sciences, Princeton University, 4 Ivy Lane, Peyton Hall, Princeton, NJ 08544, USA

⁴ Department of Astronomy, Boston University, 725 Commonwealth Ave., Boston, MA 02215 USA

have equilibrium temperatures comparable to that of the Earth, is much closer to these cool, faint stars. This increases the transit probability and number of transits per observing time baseline, thereby allowing the first detection and measurement of the occurrence of Earth-sized planets in the habitable zones of stars (Dressing & Charbonneau 2013; Quintana et al. 2014)

As a supplement to our recent efforts to characterize the lowest mass stars in the *Kepler* field (Muirhead et al. 2012a, 2014), we here focus on the transit signals in the list of M dwarf *Kepler* Objects of Interest (KOIs). Following is a uniform treatment of the sample with which we derive a statistically useful body of information regarding the properties of the planets orbiting *Kepler*'s lowest mass stars. In Section 2 we introduce the criteria that were used to define our sample and follow in Section 3 with a description of the *Kepler* data products and the preparation of these data for our following analyses. In Section 4 we outline in detail our treatment of the *Kepler* data including a preliminary characterization of the data with outlier rejection and a Markov Chain Monte Carlo parameter estimation. Also in this section we search for transit timing variations (TTVs) in the light curve data that may be due to mutual gravitational interactions within multi-planet systems or other effects, and perform custom fits to the transit shapes of those sources with significantly non-linear ephemerides. We present the full ensemble of transit candidates and stellar parameters in Section 6, and conclude in Section 7.

2. SAMPLE OF PLANET CANDIDATES

Our list of cool planet host stars is drawn from a recent *Kepler* Object of Interest (KOI) list available through the Exoplanet Archive (Akeson et al. 2013, downloaded on September 18, 2014). A total of 4228 planet transit signals toward 3250 targets were selected from the KOI list with dispositions of either “candidate” or “confirmed,” comprising a high-fidelity catalog of exoplanets (see, *e.g.* Morton & Johnson 2011; Fressin et al. 2013; Morton 2012). We choose from this list of candidates those with host star color $K_p - J > 2$ and $K_p > 14$ as a cut for M dwarfs (Mann et al. 2012). We also include 6 stars with $r - J > 2.0$ from the study by Muirhead et al. (2014) that pass our red criterion but not our faint criterion: KOI-314, KOI-641, KOI-1725, KOI-3444, KOI-3497, and KOI-4252. Lastly, we also include the new planet discovered by Muirhead et al. (2015), KOI-2704.03, or *Kepler*-445d.

We cross-match this full list with the list presented by Muirhead et al. (2014) in which near-infrared spectra for 106 stars toward 103 KOIs are presented. Two of the sources in that list are now categorized as false positives: KOI-1459 and KOI-3090. Another binary system, KOI-4463, consists of stars that appear earlier than M0 in Muirhead et al. (2014) and the KOI is not included in the Dressing & Charbonneau (2013) catalog. We leave these three targets off our list. We also exclude from further consideration a known M dwarf/white dwarf binary in the list (KOI-256 Muirhead et al. 2013), and the giant star KOI-977 (Muirhead et al. 2014). We therefore consider 98 cool KOIs from the Muirhead et al. (2014) list incorporating all 64 targets in the KOI catalog of Dressing & Charbonneau (2013), save one other now-known false positive, KOI-1164.

The newest release of KOIs postdates both the Muirhead et al. (2014) and Dressing & Charbonneau (2013) catalogs, and so we also cross matched our KOI list against the full catalog of Dressing & Charbonneau (2013) to find 9 additional cool stars with candidate transit signals: KOI-2480, KOI-2793 KOI-3102, KOI-3094, KOI-4971, KOI-4987, KOI-5228, KOI-5359, and KOI-5692. These targets are some of the smallest and longest period planet candidates in our list and offer exciting possibilities for followup observations.

The final sample we consider for further characterization consists of 167 planet signals toward 107 cool stars observed by *Kepler*. A majority of the stars in this sample (76) show single transit signals, while we find 13 double systems, 10 triple systems, 5 quadruple systems, and 3 quintuple systems. However, the majority of planet candidates, 54.5%, are in multi-transiting systems. The multi-planet systems have a higher probability of being true planetary systems due to a paucity of astrophysical false positive scenarios that could produce multiple, independent transit-like signals within a single *Kepler* aperture (*e.g.* Lissauer et al. 2014; Rowe et al. 2014) while also passing the data validation pipeline (Wu et al. 2010).

3. DATA PREPARATION

3.1. *Kepler* Data

The targets in our sample were observed over the entire course of the *Kepler* mission. However, in Quarter 0 only three cool KOI targets were observed. Over the rest of the mission an average of 87% of the targets in our sample were observed each quarter producing an average of 53,567 long cadence data per target and a total of 5.7 million long cadence photometric measurements for our sample. None of the targets on our sample were observed in short cadence mode until quarter 6 when 9.3% of the targets made the short cadence target list. This fraction rose fairly steadily for the rest of the mission up to quarter 17 when nearly 25% of the cool KOIs were observed in short cadence mode producing a total of 25.8 million short cadence data.

We obtained the light curve data through the the Barbara A. Mikulski Archive for Space Telescopes⁶ (MAST) using Data Release 21 for Quarters 0 through 14, release 20 for Quarter 15, and releases 22 and 23 for Quarters 16 and 17, respectively. For all *Kepler* data header keyword definitions, we refer the reader to the *Kepler* Archive Manual⁷. We consider only data with SAP QUALITY values equal to 0. This excludes data that were taken under non-optimal circumstances or were flagged for other reasons. On average this resulted in a rejection of about 12.5% of long cadence data per target and 6.2% of short cadence data per target.

For each KOI, both the Pre-search Data Conditioning (PDCSAP; Stumpe et al. 2012; Smith et al. 2012) and Simple Aperture Photometry (SAP) data were examined. The SAP data were cotrended using the first 5 cotrending basis vectors available through the MAST website, and then deblended using the FLFRCSP and CROWDSAP header keywords. In all cases our calibrated SAP data appeared very similar or nearly identical to the PDCSAP data and we default to using the

⁶ <https://archive.stsci.edu/kepler>

⁷ see \protect\url{http://archive.stsci.edu/kepler/manuals/archive_manual.pdf}

KOI 247 = KIC 11852982

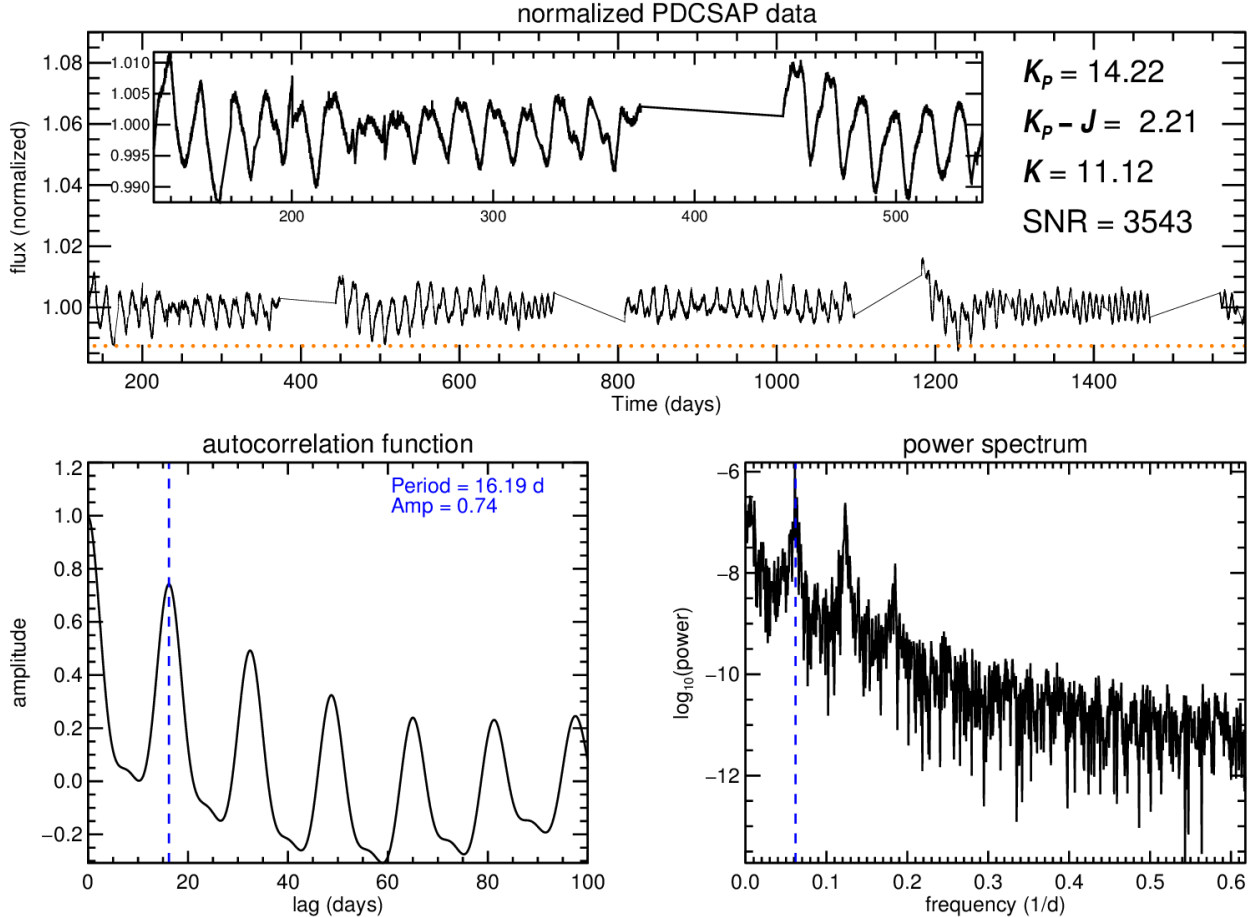


FIG. 1.— Example of a diagnostic plot for the long cadence data of KOI-247 showing the out of transit data characteristics including the signal to noise of the light curve and absolute photometry. The top panel shows the entire span of the long cadence dataset with a zoom in window of the first 400 days. The transit times are marked on the upper panel plot with colored dots (orange dots in this example) for reference. The lower panels show periodicities in the out of transit data via the autocorrelation function (lower left) and Fourier transform (lower right) from which we estimate the stellar rotation period. The vertical lines (blue, dashed) denotes the peak of the auto-correlation function and its corresponding frequency.

PDCSAP data for all KOIs for the sake of uniformity.

Before addressing the transit signals, we first look at the raw data for anomalies, trends and other potential problems. Figure 1 shows an example of one of our diagnostic plots that displays the entire time series of data, a zoom in of a small portion of the data, and photometry information. A normalized flux series is created for each KOI in our list by concatenating all available data normalized by the median flux value of each quarter. We then subtract the median flux of the combined series and blank out any transit signals using the durations and ephemerides provided by the Exoplanet Archive. These data are then gridded onto a uniform time series and zeroed at values where data were missing. Periods were searched out to 100 days using both an auto-correlation and Fourier transform. The normalized light curves, auto-correlation functions, and spectral power density were then inspected by eye. In a majority of cases where periodic signatures were seen, they are interpreted as modulations due to the combination of stellar rotation and a non-uniform stellar surface brightness.

3.2. Extracting Transit Signals

Each of the 167 planet signals described above was extracted from the full *Kepler* light curve by fitting a linear drift to the out of transit data extending two transit durations before the beginning of ingress and two durations after egress. The transit times and durations used in this process were taken from the Exoplanet Archive. Linear ephemerides were assumed for each of the transit signals in the extraction process. However, a small buffer of 10% the reported transit duration was used to account for any potential transit timing variations or errors in the values reported by the Exoplanet Archive. The root-mean-squared (rms) value of the residuals to the linear trend is recorded and applied to all the data from each transit event as the relative flux error.

Next, each transit signal was confirmed using a box-least squared algorithm (BLS; Kovács et al. 2002) optimized to oversample the projected BLS peak width by a factor of 3 (see Ofir 2014). This typically produced convincing transit signals with durations and ephemerides that were in general agreement with the values on the Exoplanet Archive. However, there were a few excep-

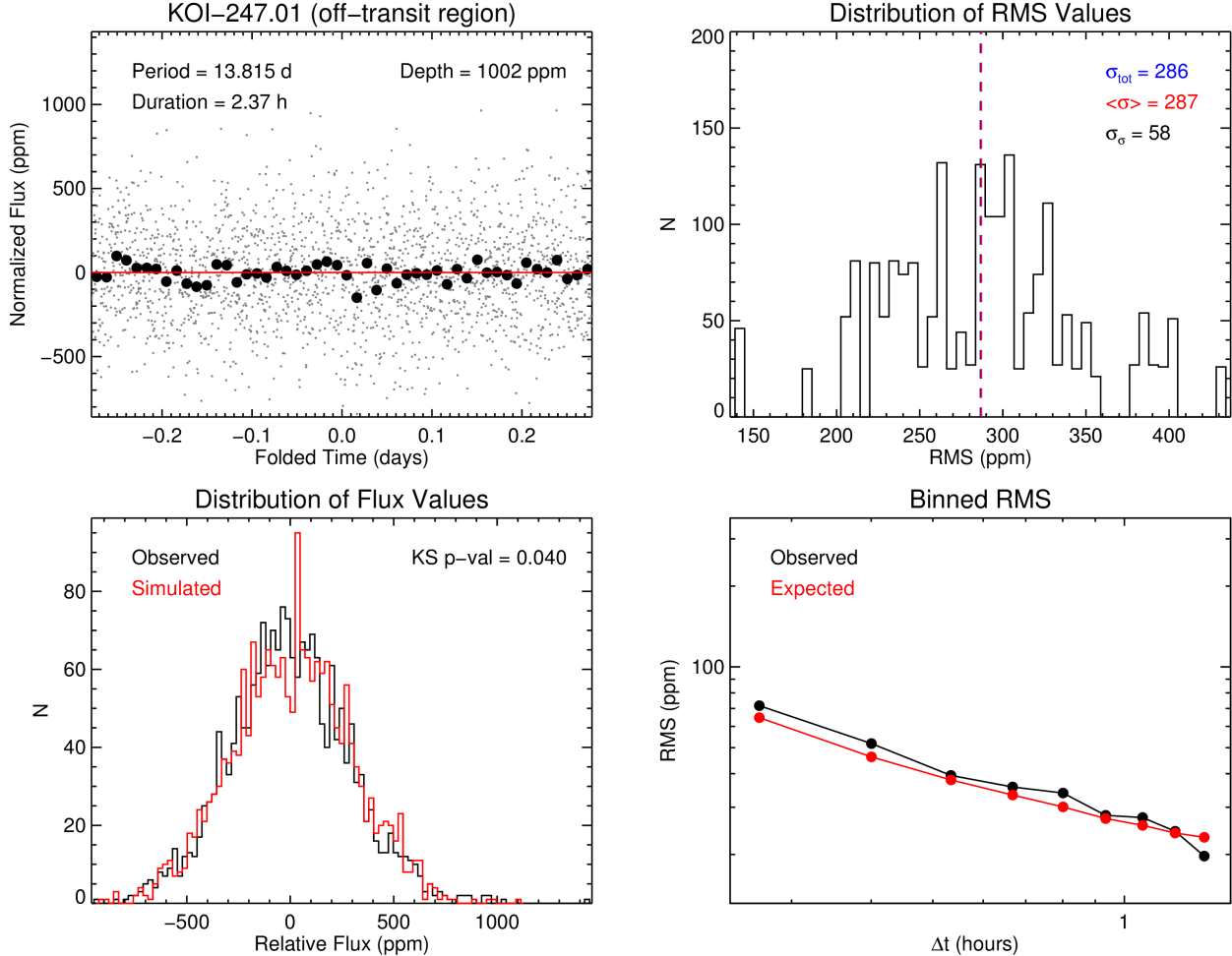


FIG. 2.— (Top left) The adjacent, transit-free section of the light curve for the specified KOI is shown folded on the period of the planet transit signal. The calibrated *Kepler* data are shown as small dots, and binned data are plotted as larger dots to reveal more subtle structure. (Top right) The distribution of RMS values derived from the detrending process are shown in histogram form. The RMS of the folded data, σ_{tot} , is depicted with the blue dotted line; the mean of the RMS values derived from the detrending process, $\langle \sigma \rangle$, is shown as the dotted red line; and the spread in the detrend derived RMS values, σ_σ , is also displayed. (Bottom left) Histogram of the data from the top left panel is shown and compared with a histogram of values drawn from a normal distribution with zero mean and a standard deviation equal to the RMS of the data. The results from a two-sided Kolmogorov-Smirnov test show the probability that the two distributions were drawn from the same parent sample. (Bottom right) The phase folded data are binned on a series of time scales, Δt , starting with the smallest bin that will include at least 20 points and stepping up in 10 bins to one half the transit duration as reported by the *Kepler* team. This curve is shown in relation to the expected trend (e.g., Winn et al. 2008)

tions. KOI-1686.01 and KOI-1408.02⁸ do not show a convincing transit signal and we hereafter leave these off of our list. Also, the period reported for KOI-1725 was found to be approximately 9 minutes off, necessitating an independent period search to adequately retrieve this signal. In cases where a transit signal was apparent in long cadence data, but problematic or not clearly seen in the short cadence data (typically due to a paucity of short cadence data), the transit parameters derived from the long cadence data were applied to the short cadence data. Examples of extracted transit signals are shown in Section 4.

Correlated noise produced by either instrumental or astrophysical phenomena can have a significant affect on the interpretation of astronomical light curve data (see, e.g. Pont et al. 2006; Carter & Winn 2009). Therefore, in addition to the transit extraction, a section of the light

⁸ We note that after the time we downloaded the KOI information from the NASA Exoplanet Archive, the disposition for KOI-1408.02 was changed to “false positive.”

curve with no transit signal was extracted in exactly the same manner as the transit signal, but according to a mid-transit time advanced by 5 times the reported transit duration. This produced a transit-free section of the light curve immediately adjacent to the extracted transit events. Figure 2 shows one example of a “blank” extraction as well as the basic analyses we use to assess the noise properties of our data (see caption for more details). We find that the distribution of data values for each KOI can be reasonably described by a single parameter, σ and compares well with synthetic, Gaussian distributed data (typical KS p-values $\gtrsim 0.01$). The fact that the noise properties of our data sample appear nearly Gaussian can be attributed to a variety of factors. A dominant effect is that the stars in our sample are by design faint, meaning that the photon noise is higher than for the rest of the sample which can mask subtler, correlated phenomena. Also, the astrophysical noise from M dwarf light curves are typically from inhomogeneities in the stellar surface brightness coupled

with stellar rotation rather than pulsation modes (see, *e.g.* Rodríguez-López et al. 2012). The stellar rotation timescales are typically much longer than the transit durations, so these effects are adequately corrected with our detrending process. We therefore do not consider the effects of correlated noise in later analyses.

A final step in the preparation of our light curves is outlier rejection. This procedure removes astrophysical (*e.g.*, flares) and instrumental effects not accounted for in the above procedures as well as points that were not adequately detrended. We reject outliers from the phase folded transit signal by binning the data into bins that are one half the integration time of the observations or with widths that contain at least 20 data points per bin. From the distribution of data points in each bin a robust estimation of the standard deviation is calculated using the median absolute deviation:

$$\text{MAD} = \text{median}(|x_i - \text{median}(\mathbf{x})|), \quad (1)$$

where the residuals are given by $\mathbf{x} = \{x_0, x_1 \dots x_n\}$. The MAD is then scaled to estimate the standard deviation assuming a Gaussian distribution so that $\sigma = 1.4826 \text{ MAD}$ and then data are rejected with absolute deviation from the median beyond a threshold $n\sigma$ where

$$n = \sqrt{2} \operatorname{erf}^{-1}(1 - \eta/N) \quad (2)$$

where N is the number of data point under consideration. Removing outliers in this manner produces a minimal effect on the statistical properties of the data by removing points that are inconsistent with the original robust estimation of the standard deviation of the sample given the sample size. We use a value of $\eta = 0.1$ which translates to $2.8 \lesssim n \lesssim 4.0$ for our dataset.

4. TRANSIT FITTING

4.1. Long and Short Cadence Fits Using a Linear Ephemeris Model

We characterize our vetted sample of 165 planets around 106 cool stars—now excluding KOI-1686.01 and KOI-1408.02—by first fitting all the long and short cadence data available with a linear ephemeris transit model using a Markov Chain Monte Carlo parameter estimation algorithm. Our light curve model uses the analytic solutions from Mandel & Agol (2002) for a quadratic stellar limb darkening law that provides a relative flux model for planet-to-star size ratio, projected separation, and limb darkening parameters. The hyper-geometric functions of those solutions need to be evaluated numerically and present a computational barrier. We therefore use a circular planet orbit to convert time into projected separation for a given period and transit duration. This allows us to side-step solving Kepler’s equation, and instead perform the transformation from time to relative separation between the star and planet with simple trigonometric functions. Under this approximation the ingress and egress of the model are exactly symmetric also halving the number of computations needed for each model call. Of course, this disallows subtle effects due to eccentric orbits to be adequately modeled and care must be taken when interpreting the derived transit duration in terms of stellar density (Seager & Mallén-Ornelas 2003; Kipping 2010b). However for our sample,

this effect can be accounted for and is expected to have a negligible effect on the derived transit parameters.

For our fits we parametrize our model with the scaled planet radius, R_p/R_\star ; the impact parameter, b ; the duration from the first to the fourth contact point of the transit, τ_{tot} ; the time of mid-transit as measured nearest to the middle of the *Kepler* light curve, t_0 ; the period, P ; and two limb-darkening parameters, q_1 and q_2 , that characterize the full range of quadratic parameter space of monotonically decreasing and positive value profiles (Kipping 2013).

Before our models can be compared to data, the effect of finite integration times must be considered (*e.g.* Kipping 2010a; Price & Rogers 2014). The *Kepler* Mission produced time series data sampled at two different intervals using a single exposure time. The exposure time (accumulated time of flux from a celestial source on a given pixel) is $t_{\text{exp}} = 6.020$ s, and for every exposure there is a fixed CCD readout time of $t_{\text{read}} = 0.519$ s. The short cadence data is made up of 9 such exposures and therefore the time between the start of successive short cadence data is $(t_{\text{exp}} + t_{\text{read}}) \times 9 = 58.849$ s. However, the time interval over which the astronomical signal is integrated is one read shorter than this, *i.e.*, $t_{\text{smooth}}^{\text{short}} = 9t_{\text{exp}} + 8t_{\text{read}} = 58.330$ s. Similarly, the long cadence data are made up of 270 integrations and therefore the time between successive integration times is $t_{\text{cadence}}^{\text{long}} = 1765.463$ s and the smoothing time $t_{\text{smooth}}^{\text{long}} = 1764.944$ s.

To account for the effects of integration time, we first calculate the planet path across the stellar disk assuming the planet is in a circular orbit using $b = a \cos(i)/R_\star$. The light curve for this planetary trajectory is oversampled and then smoothed using a uniform filter of width t_{smooth} . This is analogous the resampling procedure recommended by Kipping (2010a), and we hereafter refer to this process as resampling. The degree of resampling needed to produce an accurate model using this method will depend on the transit parameters. Therefore we numerically determine the optimal resampling for each transit candidate based on the parameters from preliminary fits enforcing an resampling of at least 5. For a grid of transit parameter values spanning the full range of R_p/R_\star and τ_{tot} in our data set, and for an impact parameter of 0 (the effect of finite integration time is most severe for low impact parameter transits), we first calculate a reference transit model resampled by a factor of 3001. We then calculate transit curves for the same set of input parameters resampled in steps of 2 from 3 to 501. The smallest resampling value that produces peak to peak discrepancies with the reference model of less than one part per million is then recorded. We then construct a grid of values from this procedure that we use to interpolate the optimal resampling values to be used for any of our targets based on their preliminary transit parameters.

We use a Bayesian framework to determine the best fit values for our 7 model parameters and their associated errors. To evaluate the likelihood, we do not resample the model at each data timestamp. Instead we phase fold the data at each trial period, P , and mid transit time, t_0 , and interpolate our resampled model to the phase folded timestamps of the data. This speeds up each

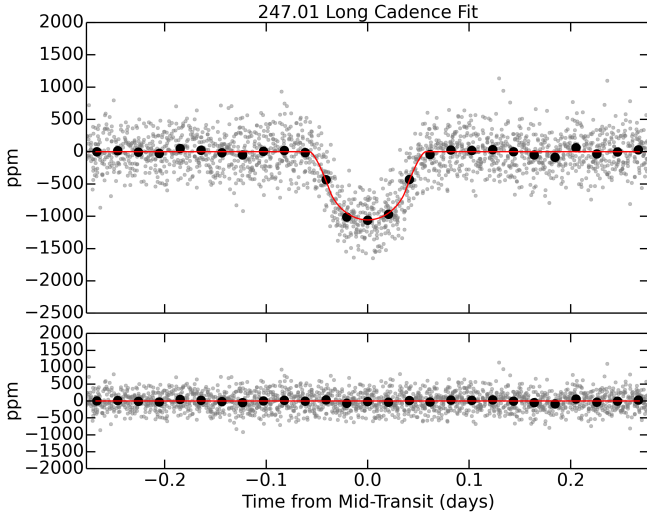


FIG. 3.— Phase folded long cadence data for KOI-247.01 are shown as gray dots. These data binned at a timescale approximately equal to the original sampling of the long cadence data stream are shown as black dots for viewing purposes only. The best fit model is shown in red and the residuals of this fit are shown in the bottom panel.

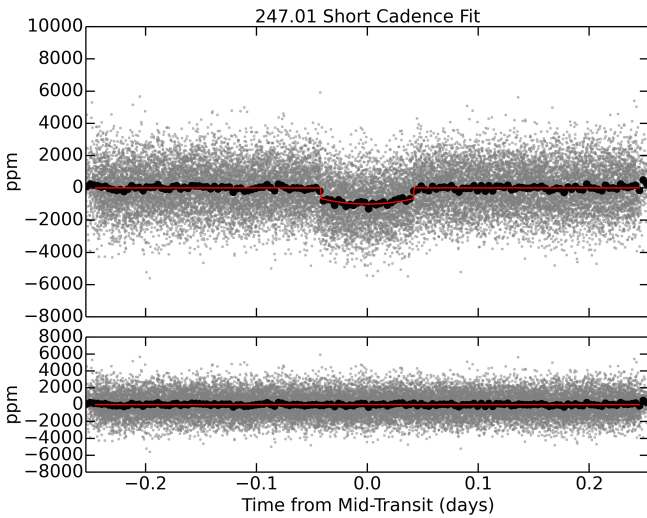


FIG. 4.— Same as Figure 3, but for the KOI-247.01 short cadence data.

likelihood call by an order of magnitude or more. The quantity $(R_p/R_*)^2$ is a scale parameter in the problem and we therefore apply a Jefferys prior to this parameter. We note that this has a small to negligible affect on our posterior samples as we are data-dominated rather than prior-dominated for the majority of our transit candidates. Each of the other free parameters have uniform priors (*i.e.*, no prior).

We use the `emcee` affine invariant Markov Chain Monte Carlo ensemble sampler (Foreman-Mackey et al. 2013) with 1000 chains, or “walkers” ($n_w = 1000$). The initial values of each walker were over-dispersed in most parameters based on the estimated values found by fitting the transit shape with a quick and flexible Levenberg-Marquardt fitting algorithm (Markwardt 2009). The relative planet radius, R_p/R_* , is dispersed in a uniform manner from 0 to a factor of 2 larger than value obtained from the preliminary fit; the full duration, τ_{tot} ,

is dispersed from half to twice the preliminary fit value; the impact parameter, b , is dispersed uniformly from 0 to 1; the period, P , is dispersed by ± 1 second from the nominal value; the mid transit times, t_0 , span 2 minutes uniformly; and the limb darkening parameters, q_1 and q_2 are dispersed uniformly between 0 and 1.

The walkers are evolved for $n_b = 1000$ steps and then analyzed. We use the correlation length, c_l , to assess if the chains have reached a sufficiently mixed state. The burn-in stage was re-run with a larger number of steps if the number of independent draws, $n_b n_w / c_l$, was found to be less than 10,000. The sampler was then reset and the walkers restarted from their last location for an additional 1000 steps. These last 1000 steps for each 1000 walkers (10^6 samples total) comprise the final posterior samples that we use to estimate the transit parameters.

The results of the long cadence data fits are summarized in Table 1, and an example fit can be seen in Figure 3. The median values for planet period, mid transit time, relative radius, duration and impact parameter are reported along with the half width of the shortest 1σ interval of the posterior for each parameter. These values are a useful reference. However, they conceal details about the probability of the these parameter values. Figure 5 shows a series of the 2-dimensional posterior probability distributions for the 7 free parameters in the fits. The expected covariance between parameters such as the impact parameter, b , and the relative size of the planet, R_p/R_* , can be clearly seen. The MCMC chains are available for download such that these parameter dependences can be properly accounted for in future statistical studies.

For 79 transit signals toward 36 cool KOIs there exist short cadence data. We follow the exact procedure outlined above for these data including preliminary fits and MCMC posterior sampling. These results are summarized in Table 2. The short cadence data fit for the same KOI shown in Figure 3, KOI-247.01, is shown in Figure 4 for reference.

4.2. Transit Timing Variations

4.2.1. TTV Search

For each transit signal we use the best-fitting transit model to fit for the times of each transit event in search of potential transit timing variations (TTVs). A single parameter, Δt_0 quantifies the time deviation of mid-transit in relation to the expected time based on a linear ephemeris from the best fits. The model light curve is fit to each transit event letting only Δt_0 float using a Levenberg-Marquardt minimization (Markwardt 2009) to produce a list of observed-minus-calculated ($O - C$) values corresponding to each transit. Figure 6 shows an example of one of the known TTV planets in our sample, KOI-248.01.

To assess the significance of potential TTV signals we first calculate the RMS scatter in the times of mid-transit as estimated by the median absolute deviation σ_{O-C} and compare that to the median value of the estimated errors on the transit times $\bar{\sigma}_{TT}$ (Mazeh et al. 2013). We consider values of $\sigma_{O-C}/\bar{\sigma}_{TT} > 3.0$ as significant. Next we compute a Lomb Normalized Periodogram⁹ for the

⁹ http://www.exelisvis.com/docs/LNP_TEST.html

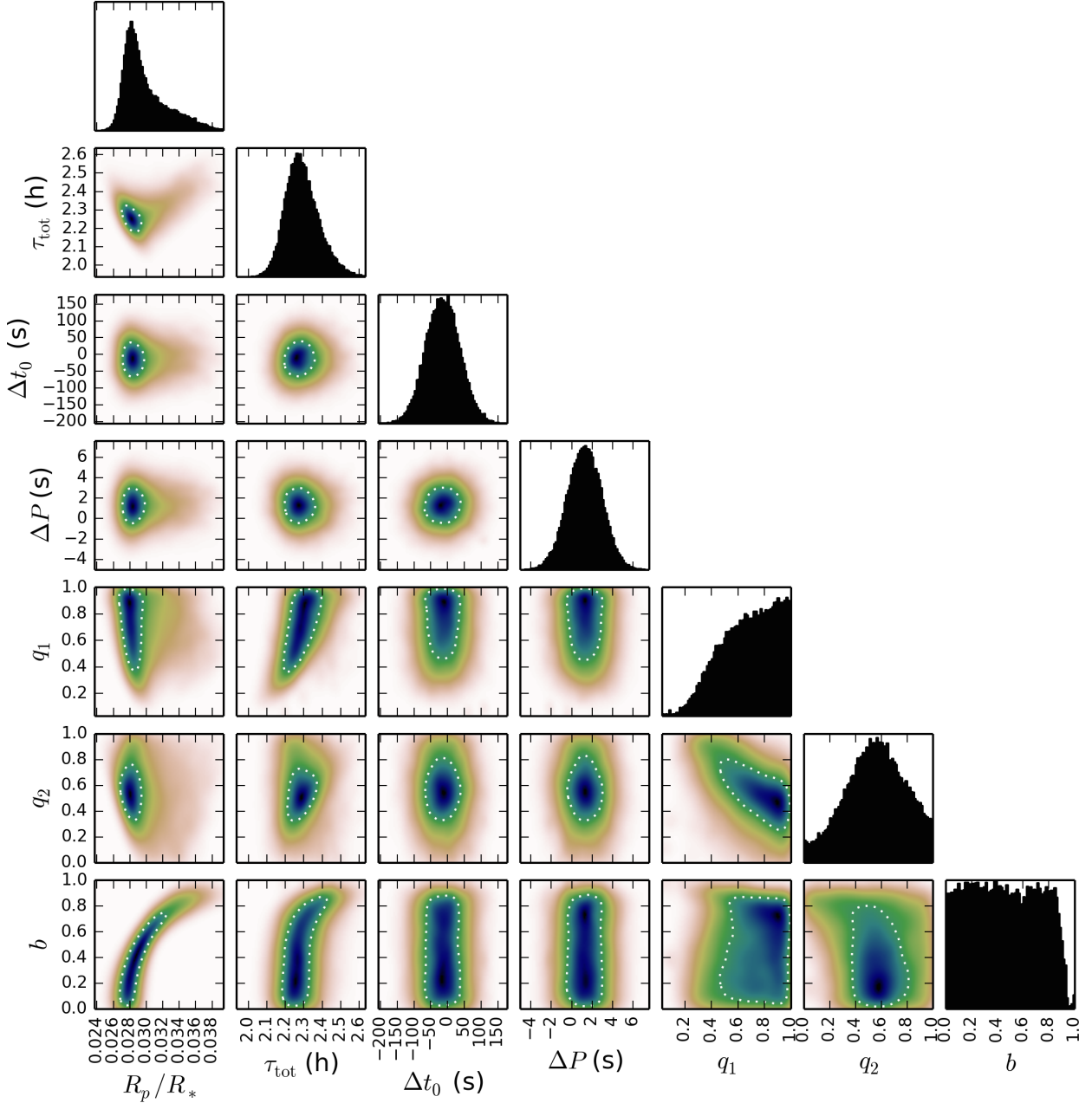


FIG. 5.— Array of 1-d and 2-d posteriors for the long cadence fit shown in Figure 3. The 2-d posteriors were constructed using a 2-d kernel density estimation that reveals covariances between parameters, most notably for R_p/R_* , b , and τ_{tot} .

calculated $O - C$ transit times. We calculate a p -value for this peak by producing 10,000 periodograms for the $O - C$ data randomly scrambled. The fractional number of periodogram peaks in the simulation that are greater than or equal to the original peak is interpreted as the probability that the measured periodogram is due to random noise, p_{LNP} . This probability value is considered significant when $p_{\text{LNP}} \leq 0.001$.

Lastly, we fit both a sine curve and a polynomial to the $O - C$ data. The sine curve model contains an amplitude, period, phase and offset. The starting parameters for the fit are a 1 minute amplitude, a period equal to the location of the peak of the periodogram, and zero phase and offset. To assess the significance of the fit results for the polynomial and sine curve models, we perform

an F-test on the fitted parameters by comparing the χ^2 values and degrees of freedom from a single parameter fit (a mean) and the polynomial or sine model. We again consider $p_{\text{sine}} \leq 0.001$ and $p_{\text{poly}} \leq 0.001$ significant.

4.2.2. TTV Results

The results were scrutinized by eye to weed out TTV signals due to stroboscopic effects and other, non-dynamical processes (Szabó et al. 2013). The results from our TTV search are summarized in Table 3. We recover 12 KOIs with significant TTV signals, 11 of which are in multi-transiting systems. These 12 planet candidates comprise 7.2% of the full M dwarf planet candidate sample and they are found toward 7 of the 106, or 6.6% of all M dwarf KOIs. All our TTV detections have been

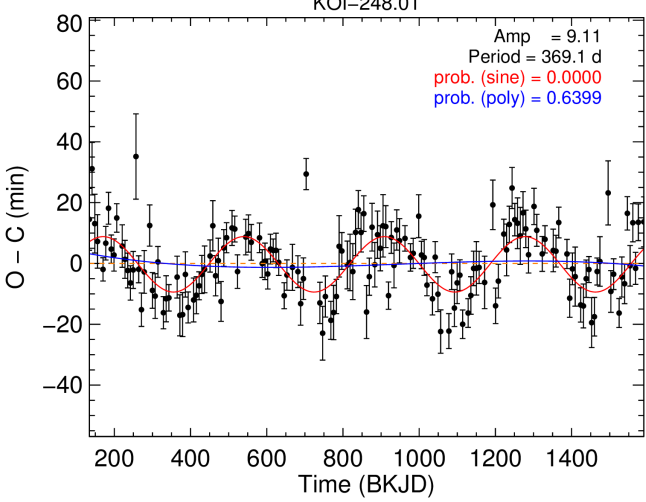


FIG. 6.— The transit timing variations ($O - C$) of KOI-248.01 fit with a pure sinusoid (red) and a polynomial (blue). These fits are only used for assessing the significance of a potential TTV signal and are not used in the fitting of the transits (see Section 4.2.3).

detected previously and are reported in the literature (Mazeh et al. 2013; Wu & Lithwick 2013; Kipping et al. 2014). However, these new transit timing results use all data from the *Kepler* mission. Following are a few notes regarding our TTV search.

KOI-3284 is reported to have a significant TTV signal by Kipping et al. (2014). Our tests show a signal at a period of ~ 190 d in both the periodogram and the sinusoid fit. However, the false alarm probability of the periodogram peak is found to be very high and this KOI also failed our F-test for the sinusoidal fit. Therefore we do not include this planet candidate in our list. KOI-2306 has $\sigma_{O-C}/\sigma_{TT} = 3.12$ due to the under sampling of the transit by the long cadence data and we therefore exclude it. KOI-1907 and KOI-2130 show some signs of long period TTV signals at ~ 700 d and ~ 1100 d periods, respectively. But both these signals fall narrowly below our selection criteria and are therefore excluded.

KOI-952.02 is not reported by Mazeh et al. (2013) as a significant TTV source. However, we find that in 17 quarters of data the periodicity at ~ 260 days is significant. This matches the period reported by Fabrycky et al. (2012). KOI-952.01 does not produce a signal significant enough to warrant inclusion in our list, though we do find that the first 8 quarters of data are consistent with the results of Fabrycky et al. (2012), and the period of ~ 260 d is apparent in our periodogram as the second highest peak but with a high formal false positive probability.

4.2.3. Fitting Transit Signals with TTVs

Transit timing variations can significantly affect the perceived transit shape under the assumption of a linear ephemeris. The effect is to essentially smear out the ingress and egress and potentially fill in the depth of the transit. The details depend on the exact nature of the TTVs. However it is typical that TTVs will bias the impact parameter to higher values, the transit duration to larger values, and the limb darkening parameters will tend toward values that produce a more severe contrast between the center of the star and the limb.

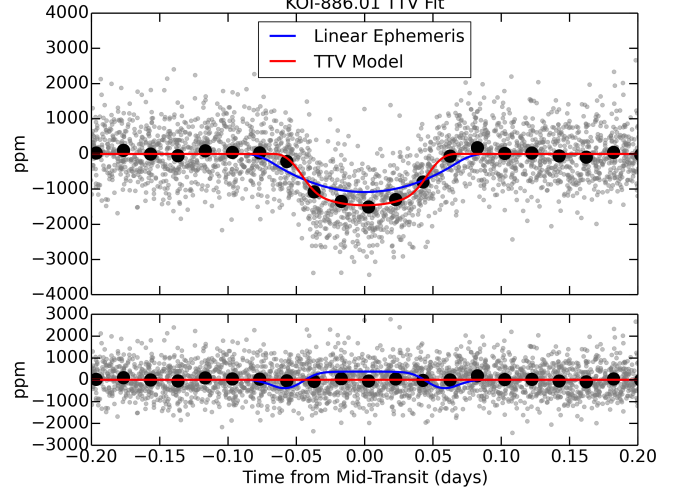


FIG. 7.— (top) Long cadence *Kepler* photometry of KOI-886.01 phase folded on the transit times derived in Section 4.2. The best fit model assuming a linear ephemeris is shown in blue, the best fit model for the data folded on the non-linear transit times is shown in red. (bottom) The residuals of the best fit non-linear model. The difference between the linear and non-linear model is shown in blue. Assuming a linear ephemeris for this target that shows peak-to-peak TTVs of ~ 2 hours significantly affect the derived transit parameters, in particular the transit duration.

Due to these effects, we refit the transit signals in our sample that show significant TTVs after folding on the individual transit times derived above. We first reject any individual transits that have mid transit time errors that are either ill defined or are larger than 2σ from the median error. We then perform a transit fit with the same model outlined in Section 4 except that instead of fitting the period and mid-transit time, we fix the individual transit times.

We choose a large TTV source, KOI-886.01, as an example showing the potential effects of fitting linear transit model to a planet that displays significant TTVs. The ~ 2 hr peak-to-peak TTVs for KOI-886.01 bias the fits toward a larger impact parameter, a smaller planet, and a longer duration. The median posterior values for the impact parameter and relative planet size are discrepant at the 0.3, and 1.2σ levels. However the derived transit durations are in disagreement with 98% confidence. These results are shown pictorially in Figure 7.

5. FALSE POSITIVE PROBABILITY

The *Kepler* pipeline is known to have produced a high fidelity sample of transiting exoplanets (Wu et al. 2010; Morton & Johnson 2011; Morton 2012; Christiansen et al. 2013; Fressin et al. 2013). Up to this point we have treated every signal as a transiting exoplanet. However, it is prudent to assign to each transit signal a probability that the signal was generated from another astrophysical scenario. We use the methods of Morton & Johnson (2011) and Morton (2012) to analyze the light curves shapes that we have extracted to assign a false positive probability (FPP) of each transit signal independently.

These FPPs are reported in Table 4 along with the probability of the transiting planet scenario compared to all other astrophysical scenarios, $P = L_{TP}/L_{FP}$; the specific occurrence assumed in the calculation, $f_{pl,specific}$; and the specific planet occurrence needed to achieve a threshold FPP of 0.005, $f_{p,V}$. Included in each calcula-

tion is also a confusion radius within which false positives are permitted to exist. For this radius we use three times the uncertainty in the multi-quarter difference-image pixel response function (PRF) fit that is reported at the Exoplanet Archive [the “PRF $\Delta\theta_{MQ}$ (OOT)” column]. The minimum exclusion radius we allow is 0.5 arcseconds, and the default value we use if no value is available is 4 arcseconds. An example of a diagnostic plot generated by the FPP analysis is shown in Figure 8.

We find that 11% of the sample, or 18 of the 165, has a FPP of larger than 10%, consistent with estimations of the entire *Kepler* sample (Morton & Johnson 2011; Fressin et al. 2013). However, 6 of these high FPP targets are either known planets in the literature (*e.g.*, KOI-254.01 (Johnson et al. 2011b), and KOI-886.02 (Steffen et al. 2013)), KOI-1422.05 (Rowe et al. 2014)) or are part of 3 or 4 transit systems much less likely to be a false positives. Therefore this is a high fidelity sample of transiting exoplanets around the lowest mass stars observed by the *Kepler* primary mission.

We do note that our treatment of exclusion radius ignores the possibility of more distant PRF contamination, as detected via the period-epoch match study of Coughlin et al. (2014), which found that “parent” eclipsing stars even up to 10-100 arcseconds from the target star were able to cause “child” false positive signals. While that work discovered over 600 false-positive KOIs, it also highlighted the possibility of further distant contaminants that might remain undetected because the “parent” may not be a known eclipsing system.

In order to estimate the rough probability of any of the present KOIs being false positives via this mechanism, we may use the numbers discussed by Coughlin et al. (2014). That work identified 12% of all known KOIs (not all planet candidates) to be from PRF contamination. However, they pointed out that only about 1/3 of the stars in the *Kepler* field were downloaded, so it might be reasonable to assume that for every discovered PRF contaminant, there might be two undiscovered, putting the overall rate at about 36%. According to this reasoning, about 24% of all KOIs might be PRF contaminants unable to be discovered by the period-epoch match method.

However, they also go on to point out that 5/6 of the FPs they detected were also identified as FPs by other methods (*e.g.*, pixel-centroid offsets, detected secondary eclipses, etc.). So this implies that of those previously mentioned 24%, only 1/6 of those, or 4% of all KOIs, might be long-distance PRF contaminants undetected by any *Kepler* FP vetting procedure and thus making it to planet candidate status. Comparing this to the ~64% of all KOIs expected to be true planets, we estimate that an additional ~6-7% of *Kepler* planet candidates, beyond what we calculate here using the methods of Morton (2012), could still be false positives. Incorporating in detail this additional long-distance PRF contamination into quantitative models of false-positive probability is thus warranted, but beyond the scope of this present work.

Additionally, we also note that the FPPs presented in this paper do not consider the number of independent transit signals in the light curve, nor the possibility of detected TTVs, both of which may substantially reduce the FPP (*e.g.*, Lissauer et al. 2014; Rowe et al. 2014;

Ford et al. 2011).

6. THE ENSEMBLE OF M DWARF PLANET CANDIDATES

The cool KOI catalog enables study of the smallest and possibly most numerous planet population discovered by *Kepler* and helps to advance our knowledge of planet formation around the most common types of stars. It is estimated that 75% of the stars within 10 pc are M dwarfs (Henry et al. 1994; Reid & Cruz 2002; Henry et al. 2004). Therefore by targeting this population we are also learning what can be expected of the closest planetary systems outside our Solar System.

To further our understanding of this sample of small planets we present uniformly derived transit parameters for all known transit signals around the cool KOIs. These stars constitute a small fraction (about 2%) of the total *Kepler* targets. However, the sample is large enough to allow for meaningful statistical analyses (Morton & Swift 2014; Ballard & Johnson 2014). Since M dwarf stars are difficult to characterize observationally, it is also important that our sample is small enough such that each individual star can be addressed with followup observations.

The planet candidates of this work have been drawn from the Exoplanet Archive list using the cool dwarf photometric cuts of Mann et al. (2012). Additional vetting was performed using near infrared, medium resolution spectroscopy (Muirhead et al. 2012b, 2014). Our final sample contains 165 planets around 106 cool stars. The number of single transit systems totals 77, while there are 11 double systems, 10 triple systems, 5 quadruple systems, and 3 quintuple systems. A total of 53.3% of these planets are found in multi-transit systems, and of these multis 11.4% show significant TTV signals. On the contrary, only one single transit system out of 77, or 1.3%, shows a significant TTV signal.

The final results of our transit fits to *Kepler* long and short cadence data are summarized in Tables 1 and 2, respectively. These tables display the results from the linear ephemeris model for all KOIs except for those listed in Table 3. For those sources we report the period, P , and mid transit time, t_0 , from the linear ephemeris fits (although it should be noted that these parameters are not strictly defined in this context) and the other transit parameters from the non-linear ephemeris fits. An earlier version of this catalog has already been used in the literature to infer statistical properties of the *Kepler* M dwarf planet population (Morton & Swift 2014), and is presented here such that it may be used for further statistical studies. Each transit signal has been treated individually, and we have generated posterior samples of the 7 transit parameters using uninformed priors that are available for download along with a suite of diagnostic plots for each KOI.

The cumulative distributions for the four transit parameters that have the most direct relevance to the planet statistics are displayed in Figure 9. For this plot and those that follow we distinguish between the planets that are in single transit and multi-transit systems.

6.1. Stellar Characteristics

The physical parameters of the transiting planets are intimately tied to the stellar parameters. We therefore also consolidate data for the stellar sample both from this work and from the literature. Stellar masses, radii

K00247.01

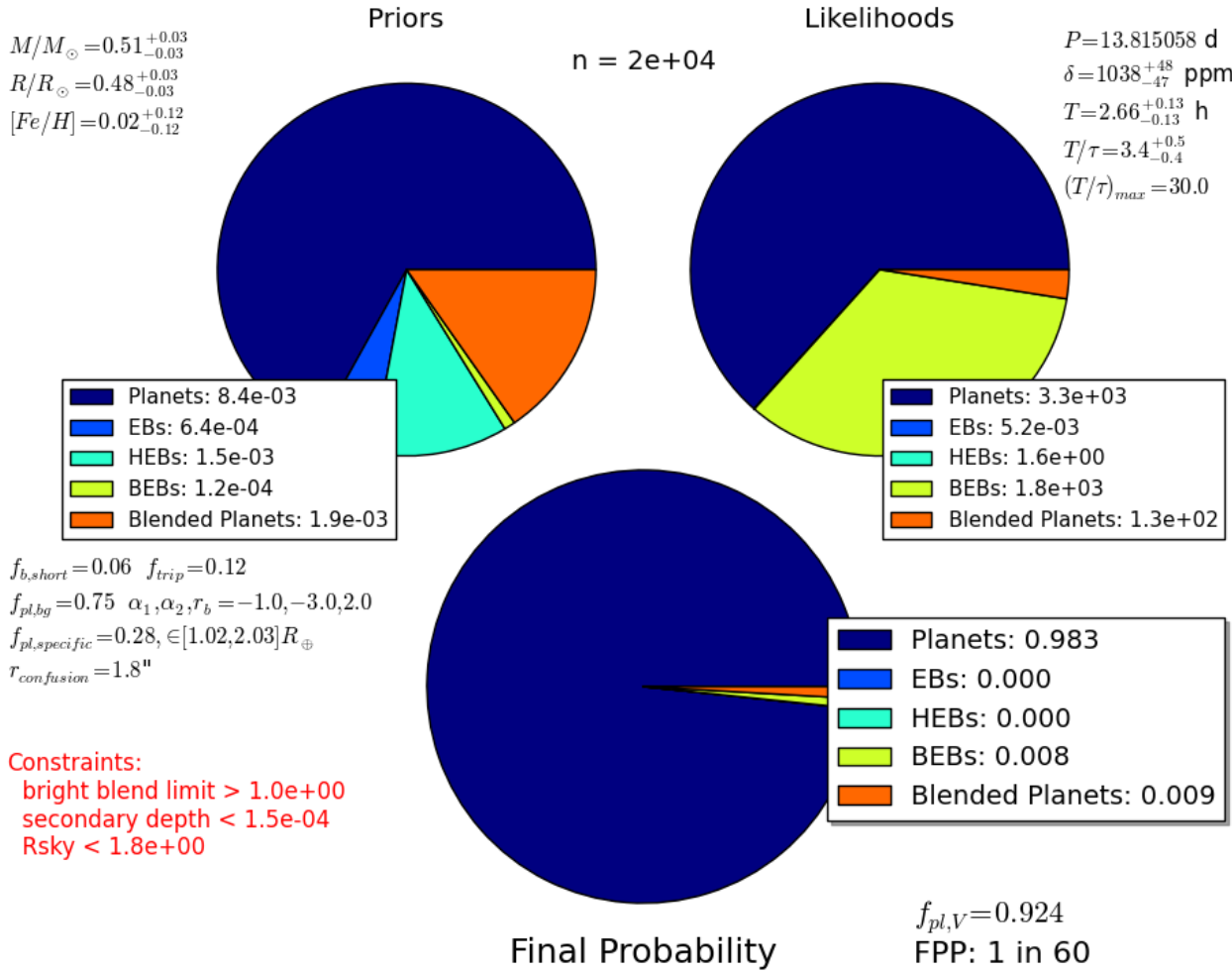


FIG. 8.— Diagnostic plot showing the key results of the false positive probability analysis for the sample of transit planet candidates around low mass stars. The top left pie chart shows the priors likelihoods of the five different scenarios considered: Transiting planet (*Planets*), eclipsing binary (*EB*), hierarchical eclipsing binary (*HEB*), background eclipsing binary (*BEB*), and blended planet. These fractions are calculated with a Galactic model in the direction of the target star with an assumed planet occurrence ($f_{pl,specific}$). The top right is the likelihood of these different scenarios given the shape of the long cadence light curve. For this case, KOI-247, the signal is most likely a transit signal around the intended star. However, the most likely false positive scenarios are background eclipsing binaries and blended planet signals.

and effective temperatures were obtained from the lists of Muirhead et al. (2014) and Dressing & Charbonneau (2013). By default we use the stellar parameters derived from the medium resolution, infrared spectroscopy of Muirhead et al. (2014). The method uses a calibrated empirical relationship between the shape of the pseudo-continuum in the K -band spectrum to infer a stellar effective temperature (H₂O-K2 index Rojas-Ayala et al. 2012). The equivalent widths of the Ca I triplet and Na I doublet within the same band are used to estimate the stellar metallicity using a relationship calibrated on nearby wide binaries with FGK type stars (Rojas-Ayala et al. 2010). The mass and radius of the star is then estimated by interpolating these T_{eff} and [M/H] values onto stellar evolutionary tracks (Dotter et al. 2008; Feiden et al. 2011).

For KOIs that do not have parameters derived with near infrared spectra, we use the stellar parameters from Dressing & Charbonneau (2013). Here the authors in-

terpolate the wide band photometry from the *Kepler* input catalog (KIC; Brown et al. 2011) onto stellar evolution models to obtain masses, radii and metallicities. The mass and radius values derived by this method are typically in reasonable agreement with Muirhead et al. (2014), while the metallicity estimates are comparatively less reliable.

These compiled values and errors are presented in Table 5 along with the photometry from the KIC. In addition to this information we also include our estimate of the stellar rotation period derived from the rotational modulation of an inhomogeneous surface brightness distribution. We are able to detect this rotational signature in a large fraction of our sample, about 86%, and report the period corresponding to the largest peak of the auto-correlation function that we validate by visual inspection. The stellar rotation period can be an important parameter in the characterization of the planet sample as this allows for age estimates (Barnes 2003) as well as activ-

Cumulative Transit Parameter Distributions

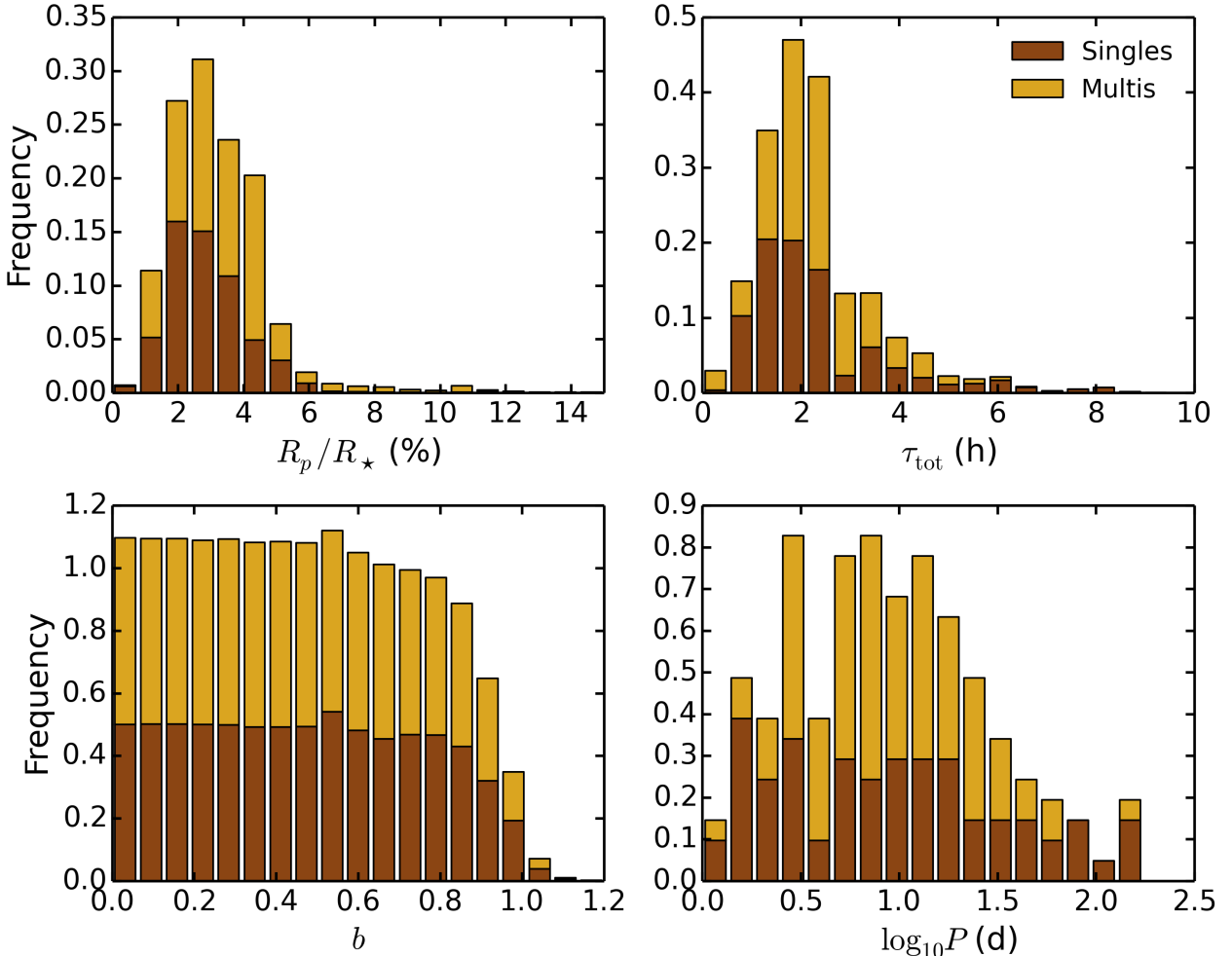


FIG. 9.— Cumulative distributions of four of the seven transit parameters for the sample of exoplanet candidates orbiting *Kepler*'s coolest dwarf stars. The radii of the planet candidates (*top left*) are displayed in terms of a percentage of the radius of the host star. The total duration (first to fourth contact point, *top right*) is shown in units of hours. The impact parameter (*bottom left*) is seen to be mostly indeterminable from the long cadence data except for KOI-254/*Kepler*-45 which accounts for the bump near $b = 0.54$. The periods of the planet candidates span more than 2 orders of magnitude and are shown on a \log_{10} scale (*bottom right*) to reveal more detail of the distribution. The stacked histograms differentiate the sample of single transit systems (brown) and planets in multi-transit systems (gold).

ity levels (e.g., Reiners et al. 2012). The distribution of stellar parameters are shown for host stars of single and multi-transit systems in Figure 10.

7. SUMMARY AND CONCLUSION

Many exciting discoveries and insights from the *Kepler* Mission have come from the relatively small sample of M dwarf stars (Muirhead et al. 2012b, 2013; Johnson et al. 2011b, 2012; Dressing & Charbonneau 2013; Morton & Swift 2014; Ballard & Johnson 2014; Quintana et al. 2014). The small sizes of these stars make it easier to probe deeper into the realm of super-Earth and terrestrial planets where planets form most readily. The cool surface temperatures facilitate detections of ever smaller planets in or near to where liquid water may exist on their surfaces due to the shorter orbital periods and higher transit probability. While this sample is a mere 2% of the total number of stars *Kepler* observed during its primary mission, it offers a glimpse into the formation of the most numerous planets orbiting the most numerous

stars in the Galaxy.

These facts have played a large role in motivating our group's efforts to understand this population of stars and planets. In this work we present a uniform analysis of the photometry of cool dwarf stars spanning the full *Kepler* primary mission the results of which are catalogs of transit parameters and stellar parameters for 165 transit candidates orbiting 106 low-mass dwarf stars. The stellar parameters are taken primarily from Muirhead et al. (2014), and supplemented with values from Dressing & Charbonneau (2013). We add new stellar rotation periods estimated directly from the *Kepler* light curves, and recover rotational modulation for nearly 86% of our targets.

As the statistical treatments of the *Kepler* data set continue to advance and improve, these transit parameters are meant to serve as a valuable dataset. To facilitate further studies we make available the posterior distributions of the transit parameters for each planet candidate

Cumulative Stellar Parameter Distributions

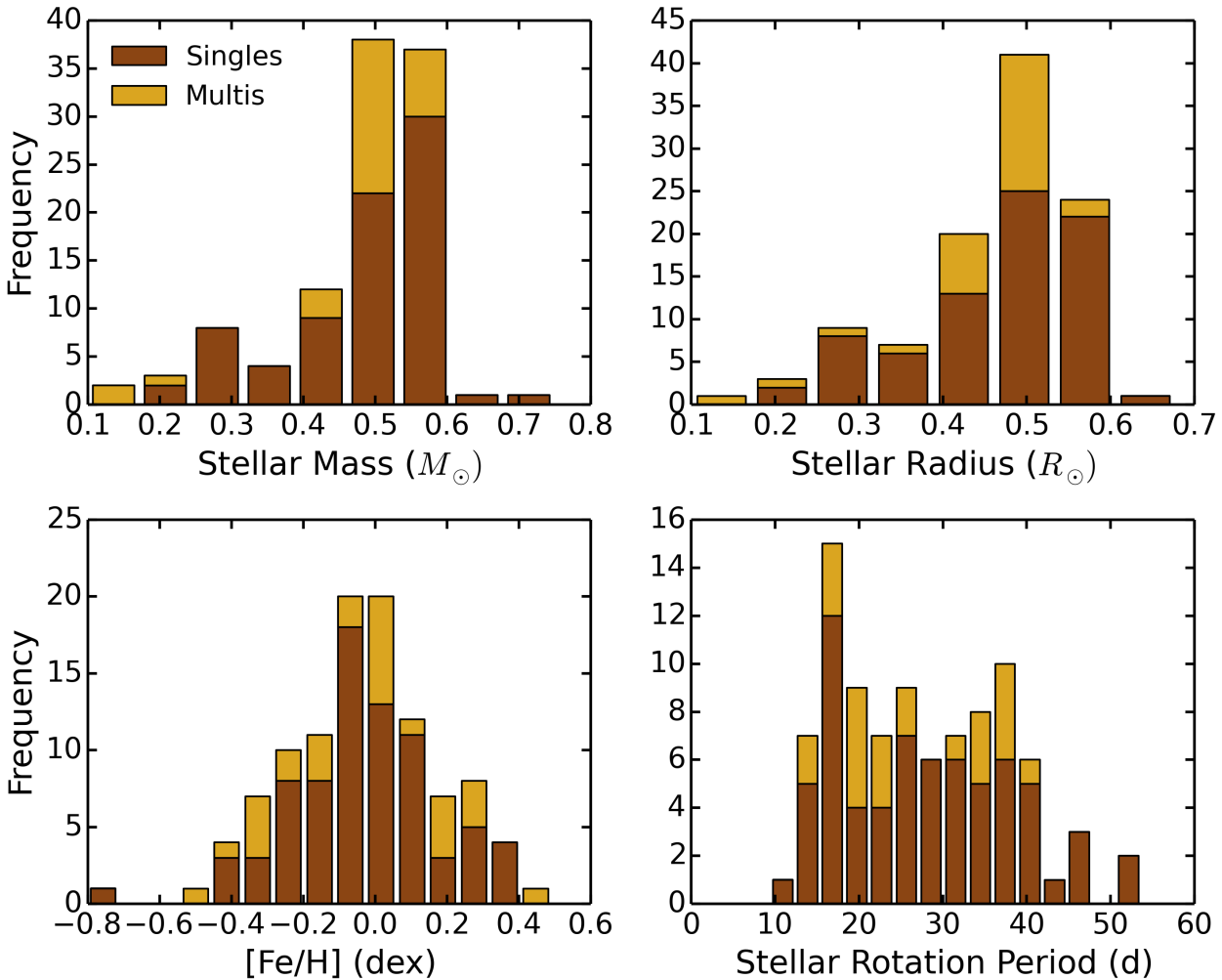


FIG. 10.— Distribution of stellar parameters for the final ensemble of 106 cool KOIs. The host stars of single transit systems and multi-transit systems have been distinguished are shown in dark and light shading, respectively.

including short cadence fit parameters where available. Diagnostic plots for each KOI created during the reduction and analysis of the light curves are also available for each star and transit.

JJS would like to thank Jason Eastman, David Kipping, Ellen Price, and Natalie Batalha for their helpful input regarding various aspects of this work. All of the data presented in this paper were obtained from the Mikulski Archive for Space Telescopes (MAST). STScI is operated by the Association of Universities for Research in Astronomy, Inc., under NASA contract NAS5-26555. Support for MAST for non-HST data is provided by the NASA Office of Space Science via grant NNX13AC07G and by other grants and contracts. This paper includes data collected by the *Kepler* mission. Funding for the *Kepler* mission is provided by the NASA Science Mission directorate. A.V. and B.T.M are supported by the National Science Foundation Graduate Research Fellowship, Grants No. DGE 1144152 and DGE 1144469, respectively.

REFERENCES

- Akeson, R. L., Chen, X., Ciardi, D., Crane, M., Good, J., Harbut, M., Jackson, E., Kane, S. R., Laity, A. C., Leifer, S., Lynn, M., McElroy, D. L., Papin, M., Plavchan, P., Ramírez, S. V., Rey, R., von Braun, K., Wittman, M., Abajian, M., Ali, B., Beichman, C., Beekley, A., Berrian, G. B., Berukoff, S., Bryden, G., Chan, B., Groom, S., Lau, C., Payne, A. N., Regelson, M., Saucedo, M., Schmitz, M., Stauffer, J., Wyatt, P., & Zhang, A. 2013, PASP, 125, 989
- Ballard, S. & Johnson, J. A. 2014, ArXiv e-prints
- Barnes, S. A. 2003, ApJ, 586, 464
- Batalha, N. M., Rowe, J. F., Bryson, S. T., Barclay, T., Burke, C. J., Caldwell, D. A., Christiansen, J. L., Mullally, F., Thompson, S. E., Brown, T. M., Dupree, A. K., Fabrycky, D. C., Ford, E. B., Fortney, J. J., Gilliland, R. L., Isaacson, H., Latham, D. W., Marcy, G. W., Quinn, S. N., Ragozzine, D., Shporer, A., Borucki, W. J., Ciardi, D. R., Gautier, III, T. N., Haas, M. R., Jenkins, J. M., Koch, D. G., Lissauer, J. J., Rapin, W., Basri, G. S., Boss, A. P., Buchhave, L. A., Carter, J. A., Charbonneau, D., Christensen-Dalsgaard, J., Clarke, B. D., Cochran, W. D., Demory, B.-O., Desert, J.-M., Devore, E., Doyle, L. R., Esquerdo, G. A., Everett, M., Fressin, F., Geary, J. C., Girouard, F. R., Gould, A., Hall, J. R., Holman, M. J., Howard, A. W., Howell, S. B., Ibrahim, K. A., Kinemuchi, K., Kjeldsen, H., Klaus, T. C., Li, J., Lucas, P. W., Meibom, S., Morris, R. L., Prša, A., Quintana, E., Sanderfer, D. T., Sasselov, D., Seader, S. E., Smith, J. C., Steffen, J. H., Still, M., Stumpe, M. C., Tarter, J. C., Tenenbaum, P., Torres, G., Twicken, J. D., Uddin, K., Van Cleve, J., Walkowicz, L., & Welsh, W. F. 2013, ApJS, 204, 24
- Batygin, K. & Morbidelli, A. 2013, AJ, 145, 1
- Borucki, W. J., Koch, D., Basri, G., Batalha, N., Brown, T., Caldwell, D., Caldwell, J., Christensen-Dalsgaard, J., Cochran, W. D., DeVore, E., Dunham, E. W., Dupree, A. K., Gautier, T. N., Geary, J. C., Gilliland, R., Gould, A., Howell, S. B., Jenkins, J. M., Kondo, Y., Latham, D. W., Marcy, G. W., Meibom, S., Kjeldsen, H., Lissauer, J. J., Monet, D. G., Morrison, D., Sasselov, D., Tarter, J., Boss, A., Brownlee, D., Owen, T., Buzasi, D., Charbonneau, D., Doyle, L., Fortney, J., Ford, E. B., Holman, M. J., Seager, S., Steffen, J. H., Welsh, W. F., Rowe, J., Anderson, H., Buchhave, L., Ciardi, D., Walkowicz, L., Sherry, W., Horch, E., Isaacson, H., Everett, M. E., Fischer, D., Torres, G., Johnson, J. A., Endl, M., MacQueen, P., Bryson, S. T., Dotson, J., Haas, M., Kolodziejczak, J., Van Cleve, J., Chandrasekaran, H., Twicken, J. D., Quintana, E. V., Clarke, B. D., Allen, C., Li, J., Wu, H., Tenenbaum, P., Verner, E., Bruhweiler, F., Barnes, J., & Prsa, A. 2010, Science, 327, 977
- Borucki, W. J., Koch, D. G., Basri, G., Batalha, N., Boss, A., Brown, T. M., Caldwell, D., Christensen-Dalsgaard, J., Cochran, W. D., DeVore, E., Dunham, E. W., Dupree, A. K., Gautier, III, T. N., Geary, J. C., Gilliland, R., Gould, A., Howell, S. B., Jenkins, J. M., Kjeldsen, H., Latham, D. W., Marcy, G. W., Lissauer, J. J., Monet, D. G., Sasselov, D., Tarter, J., Charbonneau, D., Doyle, L., Ford, E. B., Fortney, J., Holman, M. J., Seager, S., Steffen, J. H., Welsh, W. F., Allen, C., Bryson, S. T., Buchhave, L., Chandrasekaran, H., Christiansen, J. L., Ciardi, D., Clarke, B. D., Dotson, J. L., Endl, M., Fischer, D., Fressin, F., Haas, M., Horch, E., Howard, A., Isaacson, H., Kolodziejczak, J., Li, J., MacQueen, P., Meibom, S., Prsa, A., Quintana, E. V., Rowe, J., Sherry, W., Tenenbaum, P., Torres, G., Twicken, J. D., Van Cleve, J., Walkowicz, L., & Wu, H. 2011a, ApJ, 728, 117
- Borucki, W. J., Koch, D. G., Basri, G., Batalha, N., Brown, T. M., Bryson, S. T., Caldwell, D., Christensen-Dalsgaard, J., Cochran, W. D., DeVore, E., Dunham, E. W., Gautier, III, T. N., Geary, J. C., Gilliland, R., Gould, A., Howell, S. B., Jenkins, J. M., Latham, D. W., Lissauer, J. J., Marcy, G. W., Rowe, J., Sasselov, D., Boss, A., Charbonneau, D., Ciardi, D., Doyle, L., Dupree, A. K., Ford, E. B., Fortney, J., Holman, M. J., Seager, S., Steffen, J. H., Tarter, J., Welsh, W. F., Allen, C., Buchhave, L. A., Christiansen, J. L., Clarke, B. D., Das, S., Desert, J.-M., Endl, M., Fabrycky, D., Fressin, F., Haas, M., Horch, E., Howard, A., Isaacson, H., Kjeldsen, H., Kolodziejczak, J., Kulesa, C., Li, J., Lucas, P. W., Machalek, P., McCarthy, D., MacQueen, P., Meibom, S., Miquel, T., Prsa, A., Quinn, S. N., Quintana, E. V., Ragozzine, D., Sherry, W., Shporer, A., Tenenbaum, P., Torres, G., Twicken, J. D., Van Cleve, J., Walkowicz, L., Witteborn, F. C., & Still, M. 2011b, ApJ, 736, 19
- Brown, T. M., Latham, D. W., Everett, M. E., & Esquerdo, G. A. 2011, ArXiv e-prints
- Burke, C. J., Bryson, S. T., Mullally, F., Rowe, J. F., Christiansen, J. L., Thompson, S. E., Coughlin, J. L., Haas, M. R., Batalha, N. M., Caldwell, D. A., Jenkins, J. M., Still, M., Barclay, T., Borucki, W. J., Chaplin, W. J., Ciardi, D. R., Clarke, B. D., Cochran, W. D., Demory, B.-O., Esquerdo, G. A., Gautier, III, T. N., Gilliland, R. L., Girouard, F. R., Havel, M., Henze, C. E., Howell, S. B., Huber, D., Latham, D. W., Li, J., Morehead, R. C., Morton, T. D., Pepper, J., Quintana, E., Ragozzine, D., Seader, S. E., Shah, Y., Shporer, A., Tenenbaum, P., Twicken, J. D., & Wolfgang, A. 2014, ApJS, 210, 19
- Carter, J. A. & Winn, J. N. 2009, ApJ, 704, 51
- Chiang, E. & Laughlin, G. 2013, MNRAS, 431, 3444
- Christiansen, J. L., Clarke, B. D., Burke, C. J., Jenkins, J. M., Barclay, T. S., Ford, E. B., Haas, M. R., Sabale, A., Seader, S., Claiborne Smith, J., Tenenbaum, P., Twicken, J. D., Kamal Uddin, A., & Thompson, S. E. 2013, ApJS, 207, 35
- Coughlin, J. L., Thompson, S. E., Bryson, S. T., Burke, C. J., Caldwell, D. A., Christiansen, J. L., Haas, M. R., Howell, S. B., Jenkins, J. M., Kolodziejczak, J. J., Mullally, F. R., & Rowe, J. F. 2014, AJ, 147, 119
- Dotter, A., Chaboyer, B., Jevremović, D., Kostov, V., Baron, E., & Ferguson, J. W. 2008, ApJS, 178, 89
- Dressing, C. D. & Charbonneau, D. 2013, ApJ, 767, 95
- Fabrycky, D. C., Ford, E. B., Steffen, J. H., Rowe, J. F., Carter, J. A., Moorhead, A. V., Batalha, N. M., Borucki, W. J., Bryson, S., Buchhave, L. A., Christiansen, J. L., Ciardi, D. R., Cochran, W. D., Endl, M., Fanelli, M. N., Fischer, D., Fressin, F., Geary, J., Haas, M. R., Hall, J. R., Holman, M. J., Jenkins, J. M., Koch, D. G., Latham, D. W., Li, J., Lissauer, J. J., Lucas, P., Marcy, G. W., Mazeh, T., McCauliff, S., Quinn, S., Ragozzine, D., Sasselov, D., & Shporer, A. 2012, ApJ, 750, 114
- Fabrycky, D. C., Lissauer, J. J., Ragozzine, D., Rowe, J. F., Steffen, J. H., Agol, E., Barclay, T., Batalha, N., Borucki, W., Ciardi, D. R., Ford, E. B., Gautier, T. N., Geary, J. C., Holman, M. J., Jenkins, J. M., Li, J., Morehead, R. C., Morris, R. L., Shporer, A., Smith, J. C., Still, M., & Van Cleve, J. 2014, ApJ, 790, 146
- Fang, J. & Margot, J.-L. 2012, ApJ, 761, 92
- Feiden, G. A., Chaboyer, B., & Dotter, A. 2011, ApJ, 740, L25
- Ford, E. B., Rowe, J. F., Fabrycky, D. C., Carter, J. A., Holman, M. J., Lissauer, J. J., Ragozzine, D., Steffen, J. H., Batalha, N. M., Borucki, W. J., Bryson, S., Caldwell, D. A., Dunham, E. W., Gautier, III, T. N., Jenkins, J. M., Koch, D. G., Li, J., Lucas, P., Marcy, G. W., McCauliff, S., Mullally, F. R., Quintana, E., Still, M., Tenenbaum, P., Thompson, S. E., & Twicken, J. D. 2011, ApJS, 197, 2
- Foreman-Mackey, D., Hogg, D. W., Lang, D., & Goodman, J. 2013, PASP, 125, 306
- Foreman-Mackey, D., Hogg, D. W., & Morton, T. D. 2014, ApJ, 795, 64
- Fressin, F., Torres, G., Charbonneau, D., Bryson, S. T., Christiansen, J., Dressing, C. D., Jenkins, J. M., Walkowicz, L. M., & Batalha, N. M. 2013, ApJ, 766, 81
- Goldreich, P. & Schlichting, H. E. 2014, AJ, 147, 32
- Hansen, B. M. S. & Murray, N. 2012, ApJ, 751, 158

- Henry, T. J., Kirkpatrick, J. D., & Simons, D. A. 1994, AJ, 108, 1437
- Henry, T. J., Subasavage, J. P., Brown, M. A., Beaulieu, T. D., Jao, W.-C., & Hambly, N. C. 2004, AJ, 128, 2460
- Howard, A. W., Marcy, G. W., Bryson, S. T., Jenkins, J. M., Rowe, J. F., Batalha, N. M., Borucki, W. J., Koch, D. G., Dunham, E. W., Gautier, T. N., Van Cleve, J., Cochran, W. D., Latham, D. W., Lissauer, J. J., Torres, G., Brown, T. M., Gilliland, R. L., Buchhave, L. A., Caldwell, D. A., Christensen-Dalsgaard, J., Ciardi, D., Fressin, F., Haas, M. R., Howell, S. B., Kjeldsen, H., Seager, S., Rogers, L., Sasselov, D. D., Steffen, J. H., Basri, G. S., Charbonneau, D., Christiansen, J., Clarke, B., Dupree, A., Fabrycky, D. C., Fischer, D. A., Ford, E. B., Fortney, J. J., Tarter, J., Girouard, F. R., Holman, M. J., Johnson, J. A., Klaus, T. C., Machalek, P., Moorhead, A. V., Morehead, R. C., Ragozzine, D., Tenenbaum, P., Twicken, J. D., Quinn, S. N., Isaacson, H., Shporer, A., Lucas, P. W., Walkowicz, L. M., Welsh, W. F., Boss, A., Devore, E., Gould, A., Smith, J. C., Morris, R. L., Prsa, A., Morton, T. D., Still, M., Thompson, S. E., Mullally, F., Endl, M., & MacQueen, P. J. 2012, ApJS, 201, 15
- Jenkins, J. M., Caldwell, D. A., Chandrasekaran, H., Twicken, J. D., Bryson, S. T., Quintana, E. V., Clarke, B. D., Li, J., Allen, C., Tenenbaum, P., Wu, H., Klaus, T. C., Middour, C. K., Cote, M. T., McCauliff, S., Girouard, F. R., Gunter, J. P., Wohler, B., Sommers, J., Hall, J. R., Uddin, A. K., Wu, M. S., Bhavasar, P. A., Van Cleve, J., Pletcher, D. L., Dotson, J. A., Haas, M. R., Gilliland, R. L., Koch, D. G., & Borucki, W. J. 2010, ApJ, 713, L87
- Johnson, J. A., Apps, K., Gazak, J. Z., Crepp, J. R., Crossfield, I. J., Howard, A. W., Marcy, G. W., Morton, T. D., Chubak, C., & Isaacson, H. 2011a, ApJ, 730, 79
- Johnson, J. A., Gazak, J. Z., Apps, K., Muirhead, P. S., Crepp, J. R., Crossfield, I. J. M., Boyajian, T., von Braun, K., Rojas-Ayala, B., Howard, A. W., Covey, K. R., Schlawin, E., Hamren, K., Morton, T. D., & Lloyd, J. P. 2011b, ArXiv e-prints
- Johnson, J. A., Gazak, J. Z., Apps, K., Muirhead, P. S., Crepp, J. R., Crossfield, I. J. M., Boyajian, T., von Braun, K., Rojas-Ayala, B., Howard, A. W., Covey, K. R., Schlawin, E., Hamren, K., Morton, T. D., Marcy, G. W., & Lloyd, J. P. 2012, AJ, 143, 111
- Kipping, D. M. 2010a, MNRAS, 408, 1758
- . 2010b, MNRAS, 407, 301
- . 2013, MNRAS, 435, 2152
- Kipping, D. M., Nesvorný, D., Buchhave, L. A., Hartman, J., Bakos, G. Á., & Schmitt, A. R. 2014, ApJ, 784, 28
- Koch, D. G., Borucki, W. J., Basri, G., Batalha, N. M., Brown, T. M., Caldwell, D., Christensen-Dalsgaard, J., Cochran, W. D., DeVore, E., Dunham, E. W., Gautier, T. N., Geary, J. C., Gilliland, R. L., Gould, A., Jenkins, J., Kondo, Y., Latham, D. W., Lissauer, J. J., Marcy, G., Monet, D., Sasselov, D., Boss, A., Brownlee, D., Caldwell, J., Dupree, A. K., Howell, S. B., Kjeldsen, H., Meibom, S., Morrison, D., Owen, T., Reitsema, H., Tarter, J., Bryson, S. T., Dotson, J. L., Gazis, P., Haas, M. R., Kolodziejczak, J., Rowe, J. F., Van Cleve, J. E., Allen, C., Chandrasekaran, H., Clarke, B. D., Li, J., Quintana, E. V., Tenenbaum, P., Twicken, J. D., & Wu, H. 2010, ApJ, 713, L79
- Kovács, G., Zucker, S., & Mazeh, T. 2002, A&A, 391, 369
- Lissauer, J. J., Fabrycky, D. C., Ford, E. B., Borucki, W. J., Fressin, F., Marcy, G. W., Orosz, J. A., Rowe, J. F., Torres, G., Welsh, W. F., Batalha, N. M., Bryson, S. T., Buchhave, L. A., Caldwell, D. A., Carter, J. A., Charbonneau, D., Christiansen, J. L., Cochran, W. D., Desert, J.-M., Dunham, E. W., Fanelli, M. N., Fortney, J. J., Gautier, III, T. N., Geary, J. C., Gilliland, R. L., Haas, M. R., Hall, J. R., Holman, M. J., Koch, D. G., Latham, D. W., Lopez, E., McCauliff, S., Miller, N., Morehead, R. C., Quintana, E. V., Ragozzine, D., Sasselov, D., Short, D. R., & Steffen, J. H. 2011a, Nature, 470, 53
- Lissauer, J. J., Marcy, G. W., Bryson, S. T., Rowe, J. F., Jontof-Hutter, D., Agol, E., Borucki, W. J., Carter, J. A., Ford, E. B., Gilliland, R. L., Kolbl, R., Star, K. M., Steffen, J. H., & Torres, G. 2014, ArXiv e-prints
- Lissauer, J. J., Ragozzine, D., Fabrycky, D. C., Steffen, J. H., Ford, E. B., Jenkins, J. M., Shporer, A., Holman, M. J., Rowe, J. F., Quintana, E. V., Batalha, N. M., Borucki, W. J., Bryson, S. T., Caldwell, D. A., Carter, J. A., Ciardi, D., Dunham, E. W., Fortney, J. J., Gautier, III, T. N., Howell, S. B., Koch, D. G., Latham, D. W., Marcy, G. W., Morehead, R. C., & Sasselov, D. 2011b, ApJS, 197, 8
- Lithwick, Y. & Wu, Y. 2012, ApJ, 756, L11
- Mandel, K. & Agol, E. 2002, ApJ, 580, L171
- Mann, A. W., Gaidos, E., & Ansdell, M. 2013, ApJ, 779, 188
- Mann, A. W., Gaidos, E., Lépine, S., & Hilton, E. J. 2012, ApJ, 753, 90
- Markwardt, C. B. 2009, in Astronomical Society of the Pacific Conference Series, Vol. 411, Astronomical Data Analysis Software and Systems XVIII, ed. D. A. Bohlander, D. Durand, & P. Dowler, 251
- Mazeh, T., Nachmani, G., Holczer, T., Fabrycky, D. C., Ford, E. B., Sanchis-Ojeda, R., Sokol, G., Rowe, J. F., Zucker, S., Agol, E., Carter, J. A., Lissauer, J. J., Quintana, E. V., Ragozzine, D., Steffen, J. H., & Welsh, W. 2013, ApJS, 208, 16
- Morton, T. D. 2012, ApJ, 761, 6
- Morton, T. D. & Johnson, J. A. 2011, ApJ, 738, 170
- Morton, T. D. & Swift, J. 2014, ApJ, 791, 10
- Muirhead, P. S., Becker, J., Feiden, G. A., Rojas-Ayala, B., Vanderburg, A., Price, E. M., Thorp, R., Law, N. M., Riddle, R., Baranec, C., Hamren, K., Schlawin, E., Covey, K. R., Johnson, J. A., & Lloyd, J. P. 2014, ApJS, 213, 5
- Muirhead, P. S., Hamren, K., Schlawin, E., Rojas-Ayala, B., Covey, K. R., & Lloyd, J. P. 2012a, ApJ, 750, L37
- Muirhead, P. S., Johnson, J. A., Apps, K., Carter, J. A., Morton, T. D., Fabrycky, D. C., Pineda, J. S., Bottom, M., Rojas-Ayala, B., Schlawin, E., Hamren, K., Covey, K. R., Crepp, J. R., Stassun, K. G., Pepper, J., Hebb, L., Kirby, E. N., Howard, A. W., Isaacson, H. T., Marcy, G. W., Levitan, D., Diaz-Santos, T., Armus, L., & Lloyd, J. P. 2012b, ApJ, 747, 144
- Muirhead, P. S., Mann, A. W., Vanderburg, A., Morton, T. D., Kraus, A., Ireland, M., Swift, J. J., Feiden, G. A., Gaidos, E., & Gazak, J. Z. 2015, ArXiv e-prints
- Muirhead, P. S., Vanderburg, A., Shporer, A., Becker, J., Swift, J. J., Lloyd, J. P., Fuller, J., Zhao, M., Hinkley, S., Pineda, J. S., Bottom, M., Howard, A. W., von Braun, K., Boyajian, T. S., Law, N., Baranec, C., Riddle, R., Ramaprakash, A. N., Tendulkar, S. P., Bui, K., Burse, M., Chordia, P., Das, H., Dekany, R., Punnadi, S., & Johnson, J. A. 2013, ApJ, 767, 111
- Newton, E. R., Charbonneau, D., Irwin, J., & Mann, A. W. 2014, ArXiv e-prints
- Ofir, A. 2014, A&A, 561, A138
- Petigura, E. A., Howard, A. W., & Marcy, G. W. 2013a, Proceedings of the National Academy of Science, 110, 19273
- Petigura, E. A., Marcy, G. W., & Howard, A. W. 2013b, ApJ, 770, 69
- Pont, F., Zucker, S., & Queloz, D. 2006, MNRAS, 373, 231
- Price, E. M. & Rogers, L. A. 2014, ApJ, 794, 92
- Quintana, E. V., Barclay, T., Raymond, S. N., Rowe, J. F., Belmont, E., Caldwell, D. A., Howell, S. B., Kane, S. R., Huber, D., Crepp, J. R., Lissauer, J. J., Ciardi, D. R., Coughlin, J. L., Everett, M. E., Henze, C. E., Horch, E., Isaacson, H., Ford, E. B., Adams, F. C., Still, M., Hunter, R. C., Quarles, B., & Selsis, F. 2014, Science, 344, 277
- Reid, I. N. & Cruz, K. L. 2002, AJ, 123, 2806
- Rein, H. 2012, MNRAS, 427, L21
- Reiners, A., Joshi, N., & Goldman, B. 2012, AJ, 143, 93
- Rodríguez-López, C., MacDonald, J., & Moya, A. 2012, MNRAS, 419, L44
- Rojas-Ayala, B., Covey, K. R., Muirhead, P. S., & Lloyd, J. P. 2010, ApJ, 720, L113
- . 2012, ApJ, 748, 93
- Rowe, J. F., Bryson, S. T., Marcy, G. W., Lissauer, J. J., Jontof-Hutter, D., Mullally, F., Gilliland, R. L., Isaacson, H., Ford, E., Howell, S. B., Borucki, W. J., Haas, M., Huber, D., Steffen, J. H., Thompson, S. E., Quintana, E., Barclay, T., Still, M., Fortney, J., Gautier, III, T. N., Hunter, R., Caldwell, D. A., Ciardi, D. R., Devore, E., Cochran, W., Jenkins, J., Agol, E., Carter, J. A., & Geary, J. 2014, ApJ, 784, 45
- Schllichting, H. E. 2014, ApJ, 795, L15
- Seager, S. & Mallén-Ornelas, G. 2003, ApJ, 585, 1038

- Smith, J. C., Stumpe, M. C., Van Cleve, J. E., Jenkins, J. M., Barclay, T. S., Fanelli, M. N., Girouard, F. R., Kolodziejczak, J. J., McCauliff, S. D., Morris, R. L., & Twicken, J. D. 2012, PASP, 124, 1000
- Steffen, J. H., Fabrycky, D. C., Agol, E., Ford, E. B., Morehead, R. C., Cochran, W. D., Lissauer, J. J., Adams, E. R., Borucki, W. J., Bryson, S., Caldwell, D. A., Dupree, A., Jenkins, J. M., Robertson, P., Rowe, J. F., Seader, S., Thompson, S., & Twicken, J. D. 2013, MNRAS, 428, 1077
- Stumpe, M. C., Smith, J. C., Van Cleve, J. E., Twicken, J. D., Barclay, T. S., Fanelli, M. N., Girouard, F. R., Jenkins, J. M., Kolodziejczak, J. J., McCauliff, S. D., & Morris, R. L. 2012, PASP, 124, 985
- Swift, J. J., Johnson, J. A., Morton, T. D., Crepp, J. R., Montet, B. T., Fabrycky, D. C., & Muirhead, P. S. 2013, ApJ, 764, 105
- Szabó, R., Szabó, G. M., Dálya, G., Simon, A. E., Hodosán, G., & Kiss, L. L. 2013, A&A, 553, A17
- Tremaine, S. & Dong, S. 2012, AJ, 143, 94
- Winn, J. N., Holman, M. J., Torres, G., McCullough, P., Johns-Krull, C., Latham, D. W., Shporer, A., Mazeh, T., Garcia-Melendo, E., Foote, C., Esquerdo, G., & Everett, M. 2008, ApJ, 683, 1076
- Wu, H., Twicken, J. D., Tenenbaum, P., Clarke, B. D., Li, J., Quintana, E. V., Allen, C., Chandrasekaran, H., Jenkins, J. M., Caldwell, D. A., Wohler, B., Girouard, F., McCauliff, S., Cote, M. T., & Klaus, T. C. 2010, in Society of Photo-Optical Instrumentation Engineers (SPIE) Conference Series, Vol. 7740, Society of Photo-Optical Instrumentation Engineers (SPIE) Conference Series
- Wu, Y. & Lithwick, Y. 2013, ApJ, 772, 74

TABLE 1 — *Continued*

KOI	P days	δP sec	t_0 BJD-2454833	δt_0 sec	R_p/R_\star %	$\delta R_p/R_\star$ %	τ_{tot} hrs	$\delta \tau_{\text{tot}}$ min	b	δb
3444.01	12.671432	7.52	847.109778	244.33	1.255	0.114	2.4624	12.456	0.45	0.32
3444.02	60.326670	4.07	868.978213	29.89	4.570	0.485	1.5192	4.032	0.33	0.25
3444.03	2.635964	1.19	862.475680	193.79	0.872	0.086	1.5816	9.936	0.46	0.32
3444.04	14.150370	8.37	863.133061	260.69	1.213	0.137	1.6656	12.744	0.47	0.33
3497.01	20.359756	5.97	867.240981	136.49	1.678	0.143	1.9320	9.432	0.47	0.33
3749.01	10.727244	3.98	862.355778	12.88	33.313	7.429	1.8216	4.104	0.86	0.12
4087.01	101.111348	74.45	822.187936	293.50	2.948	0.131	8.0280	16.416	0.45	0.31
4252.01	15.571357	7.80	852.867242	212.30	1.198	0.121	2.1624	12.672	0.43	0.31
4290.01	4.838142	5.92	725.403809	113.76	4.608	0.356	1.2768	7.056	0.45	0.31
4427.01	147.661340	110.88	834.602096	381.92	3.205	0.242	6.1056	19.944	0.44	0.30
4875.01	0.912184	0.49	860.639395	207.27	1.211	0.140	1.1304	11.232	0.47	0.33
4971.01	146.351327	619.28	958.058444	2571.99	2.103	1.932	6.0264	121.248	0.49	0.34
4987.01	12.575041	10.14	973.068664	283.83	2.657	0.196	3.3216	15.120	0.48	0.33
5228.01	546.308421	2544.13	880.576696	3993.63	2.498	0.458	33.4776	310.896	0.54	0.36
5359.01	2.719980	15.28	584.858626	256.01	2.782	0.254	2.0352	12.312	0.46	0.33
5692.01	2.641814	1.63	861.672624	244.57	0.755	0.071	2.3208	13.680	0.45	0.32

† Transit parameters derived from fits to individual transit times. Period and mid-transit time values are taken from fits assuming a linear ephemeris.

TABLE 2 — *Continued*

KOI	P days	δP sec	t_0 BJD-2454833	δt_0 sec	R_p/R_\star %	$\delta R_p/R_\star$ %	τ_{tot} hrs	$\delta \tau_{\text{tot}}$ min	b	δb
2842.02	5.149012	28.02	1575.019753	120.10	5.350	0.592	0.8496	5.544	0.45	0.32
2842.03	3.036240	16.95	1573.224473	232.62	4.131	2.542	1.0080	12.168	0.47	0.33

† Transit parameters derived from fits to individual transit times. Period and mid-transit time values are taken from fits assuming a linear ephemeris.

TABLE 3
M DWARF PLANETS WITH TRANSIT TIMING VARIATIONS

KOI	N	$\sigma_{O-C}/\bar{\sigma}_{TT}$	LNP amp.	p_{LNP}	sine amp. (min)	P_{TTV} (days)	p_{sine}	p_{poly}
248.01	159	2.19	29.15	0.0001	9.71	365.97	0.00000	0.68916
248.02	100	2.08	7.25	0.0009	15.06	365.76	0.00383	0.42931
250.01	95	1.86	22.62	0.0001	9.76	743.74	0.00000	0.03606
250.02	52	1.63	9.38	0.0009	7.60	809.02	0.00007	0.18420
314.01	71	1.85	12.29	0.0001	5.46	1111.01	0.00000	0.00000
314.02	50	1.88	14.91	0.0001	13.86	1022.36	0.00000	0.00000
314.03	117	1.56	5.93	0.2357	32.43	1402.62	0.00008	0.00031
463.01	59	1.32	9.28	0.0021	3.65	314.51	0.00025	0.94999
886.01	158	1.82	43.24	0.0001	57.79	818.59	0.00000	0.06058
886.02	99	1.66	22.35	0.0001	105.95	871.50	0.00000	0.00706
898.01	123	0.89	7.37	0.0579	7.37	334.12	0.00060	0.86390
952.02	103	1.15	11.27	0.0001	17.61	261.62	0.00012	0.13167

TABLE 4
 FALSE POSITIVE PROBABILITY RESULTS

KOI	FPP	<i>P</i>	$f_{p,specific}$	$f_{p,V}$
247.01	0.0165	215	0.276	0.92400
248.01 ^{†‡}	0.0000	290321	0.218	0.00069
248.02 ^{†‡}	0.0902	39	0.258	5.08000
248.03 [‡]	0.0004	8541	0.276	0.02330
248.04 [‡]	0.0018	1998	0.276	0.09960
249.01	0.0000	848734	0.269	0.00023
250.01 ^{†‡}	0.0940	64	0.149	3.08000
250.02 ^{†‡}	0.0069	707	0.202	0.28200
250.03 [‡]	0.0003	10975	0.276	0.01820
250.04 [‡]	0.0030	1432	0.229	0.13900
251.01 [‡]	0.0003	17497	0.195	0.01140
251.02 [‡]	0.0036	997	0.276	0.20000
252.01	0.0018	2685	0.202	0.07400
253.01 [‡]	0.0122	428	0.189	0.46500
253.02 [‡]	0.0012	3041	0.276	0.06570
254.01	0.3690	171	0.010	1.20000
255.01 [‡]	0.0011	4614	0.195	0.04320
255.02 [‡]	0.0213	166	0.276	1.20000
314.01 ^{†‡}	0.0000	162471	0.276	0.00123
314.02 ^{†‡}	0.0000	86675	0.276	0.00230
314.03 ^{†‡}	0.0069	520	0.276	0.38300
463.01 [†]	0.0000	842598	0.276	0.00024
478.01	0.0000	91416	0.226	0.00218
531.01	0.4820	23	0.046	8.49000
571.01 [‡]	0.0002	14547	0.276	0.01370
571.02 [‡]	0.0000	241542	0.276	0.00082
571.03 [‡]	0.0000	88366	0.276	0.00226
571.04 [‡]	0.0014	2495	0.276	0.08000
571.05 [‡]	0.0046	787	0.276	0.25300
596.01	0.0000	355210	0.276	0.00056
641.01	0.0026	1406	0.276	0.14200
739.01	0.0001	54976	0.276	0.00363
781.01	0.0104	511	0.186	0.39000
812.01 [‡]	0.0000	117784	0.227	0.00169
812.02 [‡]	0.0001	64936	0.238	0.00307
812.03 [‡]	0.0001	50413	0.241	0.00395
812.04 [‡]	0.0098	366	0.276	0.54400
817.01 [‡]	0.0003	15136	0.258	0.01320
817.02 [‡]	0.0136	262	0.276	0.75700
818.01	0.0001	29391	0.233	0.00677
854.01	0.0002	22853	0.250	0.00871
886.01 ^{†‡}	0.0269	136	0.265	1.46000
886.02 ^{†‡}	1.0000	0	0.276	Inf
886.03 [‡]	0.0109	328	0.276	0.60700
898.01 ^{†‡}	0.0001	49290	0.207	0.00404
898.02 [‡]	0.0000	154069	0.266	0.00129
898.03 [‡]	0.0004	11540	0.244	0.01720
899.01 [‡]	0.0000	128024	0.276	0.00155
899.02 [‡]	0.0001	32059	0.276	0.00622
899.03 [‡]	0.0001	38377	0.276	0.00519
936.01 [‡]	0.0000	412281	0.231	0.00048
936.02 [‡]	0.0000	126681	0.276	0.00157
947.01	0.0000	578234	0.251	0.00034
952.01 [‡]	0.0006	6507	0.243	0.03060
952.02 ^{†‡}	0.0268	145	0.249	1.36000
952.03 [‡]	0.0012	3900	0.217	0.05100
952.04 [‡]	0.0141	253	0.276	0.78400
952.05 [‡]	0.0240	147	0.276	1.35000
961.01 [‡]	0.0119	300	0.276	0.66200
961.02 [‡]	0.0052	691	0.276	0.28800
961.03 [‡]	0.0424	81	0.276	2.44000
1078.01 [‡]	0.0000	102712	0.266	0.00194
1078.02 [‡]	0.0019	2155	0.249	0.09260
1078.03 [‡]	0.0046	881	0.247	0.22500
1085.01	0.0011	3414	0.276	0.05830
1141.01	0.0002	163390	0.276	0.01210
1146.01	0.0028	1272	0.276	0.15700
1201.01	0.0024	1499	0.276	0.13300
1393.01	0.0150	290	0.226	0.68500

TABLE 4 — *Continued*

KOI	FPP	P	$f_{p,specific}$	$f_{p,V}$
1397.01	0.0058	712	0.242	0.28000
1408.01	0.0025	1445	0.276	0.13800
1422.01 [‡]	0.0000	118789	0.276	0.00168
1422.02 [‡]	0.0001	35517	0.276	0.00561
1422.03 [‡]	0.0051	701	0.276	0.28400
1422.04 [‡]	0.0061	592	0.276	0.33600
1422.05 [‡]	0.1740	17	0.276	11.60000
1427.01	0.0001	31230	0.276	0.00640
1649.01	0.1800	16	0.276	12.10000
1681.01 [‡]	0.7360	1	0.276	153.00000
1681.02 [‡]	0.0089	403	0.276	0.49300
1681.03 [‡]	0.0182	195	0.276	1.02000
1702.01	0.0073	491	0.276	0.40600
1725.01	0.0007	5536	0.271	0.03590
1843.01 [‡]	0.0181	196	0.276	1.01000
1843.02 [‡]	0.0122	293	0.276	0.67700
1867.01 [‡]	0.0047	770	0.276	0.25900
1867.02 [‡]	0.0155	233	0.272	0.85500
1867.03 [‡]	0.0024	1493	0.276	0.13400
1868.01	0.0020	1994	0.249	0.09990
1879.01	0.0782	90	0.130	2.19000
1880.01	0.0009	4071	0.276	0.04890
1902.01	0.9340	0	0.254	719.00000
1907.01	0.0005	8143	0.268	0.02440
2006.01	0.0017	2153	0.276	0.09230
2036.01 [‡]	0.0336	104	0.276	1.91000
2036.02 [‡]	0.0215	164	0.276	1.21000
2057.01	0.0086	419	0.276	0.47500
2058.01	0.0032	1121	0.276	0.17700
2090.01	0.0036	1043	0.266	0.19100
2130.01	0.0045	846	0.262	0.23500
2156.01	0.0732	48	0.260	4.08000
2179.01 [‡]	0.0023	1592	0.270	0.12500
2179.02 [‡]	0.0281	125	0.276	1.59000
2191.01	0.1180	27	0.276	7.38000
2238.01	0.0069	522	0.276	0.38100
2306.01	0.0107	334	0.276	0.59500
2329.01	0.1120	28	0.276	6.93000
2347.01	0.0063	572	0.276	0.34800
2417.01	0.1860	15	0.276	12.50000
2418.01	0.0125	286	0.276	0.69600
2453.01	0.0267	132	0.276	1.51000
2480.01	0.0878	37	0.276	5.30000
2542.01	0.0079	455	0.276	0.43700
2626.01	0.0392	88	0.276	2.24000
2650.01 [‡]	0.0072	501	0.276	0.39700
2650.02 [‡]	0.0703	47	0.276	4.16000
2662.01	0.0071	504	0.276	0.39500
2704.01 [‡]	0.0011	5920	0.148	0.03360
2704.02 [‡]	0.0014	2814	0.259	0.07030
2704.03 [‡]	0.9600	0	0.276	1320.00000
2705.01	0.0001	26834	0.276	0.00741
2715.01 [‡]	0.0562	218	0.077	0.91700
2715.02 [‡]	0.0089	486	0.228	0.40900
2715.03 [‡]	0.0071	572	0.244	0.34700
2764.01	0.0005	6583	0.276	0.03030
2793.01 [‡]	0.0009	4685	0.232	0.04250
2793.02 [‡]	0.0076	475	0.276	0.41900
2839.01	0.0011	3382	0.276	0.05890
2842.01 [‡]	0.0001	32059	0.276	0.00622
2842.02 [‡]	0.0177	201	0.276	0.99100
2842.03 [‡]	0.0005	6977	0.276	0.02850
2845.01	0.0002	19268	0.276	0.01030
2862.01	0.0193	184	0.275	1.07000
2926.01 [‡]	0.0005	10656	0.193	0.01860
2926.02 [‡]	0.0014	3188	0.232	0.06250
2926.03 [‡]	0.0049	1145	0.178	0.17400
2926.04 [‡]	0.0004	11417	0.206	0.01740
2992.01	0.3460	8	0.233	24.60000
3010.01	0.0026	1422	0.275	0.14000
3034.01	0.0039	935	0.276	0.21300
3094.01	0.0183	194	0.276	1.02000

TABLE 4 — *Continued*

KOI	FPP	P	$f_{p,specific}$	$f_{p,V}$
3102.01	0.0214	165	0.276	1.20000
3119.01	0.0014	2495	0.276	0.07980
3140.01	0.2620	10	0.276	19.60000
3144.01	0.0007	5553	0.276	0.03590
3263.01	0.7140	16	0.024	11.80000
3282.01	0.0008	4860	0.243	0.04090
3284.01	0.0078	457	0.276	0.43500
3414.01	0.9620	13	0.003	17.30000
3444.01 [‡]	0.0046	777	0.276	0.25600
3444.02 [‡]	0.4130	6	0.211	29.60000
3444.03 [‡]	0.0370	94	0.276	2.11000
3444.04 [‡]	0.0416	83	0.276	2.38000
3497.01	0.0001	31230	0.276	0.00637
3749.01	0.8550	14	0.012	14.30000
4087.01	0.0004	8442	0.276	0.02360
4252.01	0.0124	288	0.276	0.69000
4290.01	0.0238	148	0.276	1.34000
4427.01	0.0636	54	0.268	3.62000
4875.01	0.0022	1635	0.276	0.12200
4971.01	0.0705	47	0.276	4.17000
4987.01	0.0118	303	0.276	0.65900
5228.01	0.8530	0	0.276	320.00000
5359.01	0.0006	6109	0.274	0.03260
5692.01	0.0124	288	0.276	0.68900

[†] Source of significant TTV signal.[‡] Multi-transit candidate system.

